Co-option of Membrane Wounding Enables Virus Penetration into Cells

Stefania Luisoni [1, 2], Maarit Suomalainen [1], Karin Boucke [1], Lukas B. Tanner [3, 8], Markus R. Wenk [3], Xue Li Guan [4], Michal Grzybek [5,6], Ünal Coskun [5,6] and Urs F. Greber[1,7]

[1] Institute of Molecular Life Sciences, University of Zurich, Winterthurerstrasse 190, CH-8057 Zurich, Switzerland

[2] Molecular Life Sciences Graduate School, ETH and University of Zurich, CH-8057 Zurich, Switzerland

[3] Department of Biochemistry, Yong Loo Lin School of Medicine, National University of Singapore, 28 Medical Drive, Singapore 117456, Singapore

[4] Swiss Tropical and Public Health Institute, Socinstrasse 57, 4051 Basel, and University of Basel, CH-4000 Basel, Switzerland

[5] Paul Langerhans Institute Dresden of the Helmholtz Centre Munich at the University Clinic Carl Gustav Carus, TU Dresden, 01307 Dresden, Germany

[6] German Center for Diabetes Research (DZD e.V.), 85764 Neuherberg, Germany

[7] corresponding author: E-mail: urs.greber@imls.uzh.ch, Telephone: +41 44 635 48 41, Fax: +41 44 635 68 17

[8] present address: Lewis-Sigler Institute for Integrative Genomics, Princeton University, Washington Road, Princeton, NJ 08544, USA

Running title: Co-option of Membrane Wounding for Virus Entry

Summary

During cell entry, non-enveloped viruses undergo partial uncoating to expose membrane-lytic proteins for gaining access to the cytoplasm. We report that adenovirus uses membrane piercing to induce and hijack cellular wound removal processes that facilitate further membrane disruption and infection. Incoming adenovirus stimulates calcium influx and lysosomal exocytosis, a membrane repair mechanism resulting in release of acid sphingomyelinase (ASMase) and degradation of sphingomyelin to ceramide lipids in the plasma membrane. Lysosomal exocytosis is triggered by small plasma membrane lesions induced by the viral membrane lytic protein-VI, which is exposed upon mechanical cues from virus receptors, followed by virus endocytosis into leaky endosomes. Chemical inhibition or RNA interference of ASMase slows virus endocytosis, inhibits virus escape to the cytosol, and reduces infection. Ceramide enhances binding of protein-VI to lipid membranes and protein-VI induced membrane-rupture. Thus, adenovirus uses a positive feedback loop between virus uncoating and lipid signaling for efficient membrane penetration.

Introduction

Insults to plasma membrane integrity are life-threatening to cells. They occur by mechanical stress, for example in muscle cells, or by pore forming proteins in bacterially intoxicated cells (Vadia et al., 2011; Walev et al., 2001). Breaching cellular membrane integrity gives rise to infectious disease and cancer, for example when microbes or viruses deliver toxins or nucleic acids into eukaryotic cells, or break down the sterility of the cytoplasm, as shown for human papillomavirus 16 (Schelhaas et al., 2012). Membrane wounding is also a crucial process in cell-based immunity, where cytotoxic T lymphocytes form pores in the plasma membrane of diseased cells and eliminate these cells by delivery of death inducing proteases (Keefe et al., 2005).

Membrane wounds of limited size can be resolved by repair processes reducing plasma membrane tension, formation of intracellular vesicle patches, removal of the lesion by endocytosis, or shedding processes (Jimenez et al., 2014; Reddy et al., 2001; Tam et al., 2010). In many cell types, membrane repair involves exocytosis of secretory lysosomes, which have additional key physiological functions in bone resorption and cytotoxicity of killer T cells against infected cells (Andrews et al., 2014; Settembre and Ballabio, 2014). Secretory lysosomes have not been implicated in early steps of viral infections so far.

Viruses depend on cellular cues for infectious entry into cells. Many enveloped viruses fuse their lipid membrane with endosomal membranes by low pH cues, or the plasma membrane by receptor-triggered conformational changes (Cossart and Helenius, 2014). These viruses do not cause membrane damage. In contrast, non-enveloped viruses enter the cytosol by membrane rupture or piercing processes depending on viral and cellular factors (Browning et al., 2012; Suomalainen and Greber, 2013). Non-enveloped viruses are wide-spread food and water-borne pathogens, and affect healthy and immune-suppressed individuals. For example, human immune-suppression leads to mortality from adenovirus viremia (Ganzenmueller et al., 2011; Matthes-Martin et al., 2013). Adenoviruses also cause strong innate and inflammatory responses, which renders them powerful gene therapy vehicles in cancer and vaccination therapies (Ewer et al., 2013; Hendrickx et al., 2014).

But how non-enveloped viruses rupture host membranes is poorly understood. Initial studies with human adenovirus species C (HAdV-C), such as HAdV-C2 or C5, showed that membrane rupture is tightly coupled to dynamin-dependent virus endocytosis and uncoating. Uncoating requires mechanical cues from virus receptor binding and leads to the exposure of the membrane lytic protein-VI (Burckhardt et al., 2011; Greber et al., 1996; Meier et al., 2002; Wiethoff et al., 2005; Wodrich et al., 2010). Subsequent penetration of endosomal membranes is independent of low endosomal pH, and does not involve virus passage through Rab7-containing endosomes (Gastaldelli et al., 2008; Suomalainen et al., 2013), although it requires host factors regulating early to late endosome maturation (Zeng and Carlin, 2013). Here we resolve this conundrum by showing that secretory lysosomes provide critical lipid cues for a two-step activation process of the viral membrane lytic protein-VI.

Results

Incoming virus triggers ceramide production through acid sphingomyelinase

Using mass spectrometry, we quantified 159 membrane lipid species during early steps in adenovirus infection of HeLa cells. Only two ceramide species were significantly up-regulated (log2 fold change > 0.4 and p-values < 0.05) at 30 min after infection with HAdV-C2. Ceramide remodeling was induced by wild type adenovirus but not by HAdV-C2-TS1 (short TS1, Fig. 1A, Supplemental Data Tab. 1). TS1 has a point mutation in the viral protease, engages with the coxsackievirus adenovirus receptor (CAR) and the co-receptor integrins akin to wild type HAdV-C2, but fails to uncoat and cross the endosomal membrane (Burckhardt et al., 2011; Gastaldelli et al., 2008; Nakano et al., 2000). Ceramides are essential structural components of membranes. They are involved in membrane signalling from microdomains, the formation of vesicles or cell death (Gault et al., 2010).

To identify the critical ceramide biosynthesis pathway activated by incoming HAdV, we used inhibitors targeting ceramide formation in the *de novo* or the salvage pathways (He et al., 2004; Wang et al., 1991), and inhibitors blocking sphingomyelin (SM) degradation by neutral and acid sphingomyelinases (Kornhuber et al., 2008; Luberto et al., 2002) (Fig. 1B). The latter enzymes convert SM to ceramide, a cone-shaped signaling lipid lacking a hydrophilic head (Bi et al., 1995). Solely, the

inhibition or silencing of acid sphingomyelinase (ASMase) reduced infection of A549 or HeLa cell lines, or primary human nasal epithelial cells with adenovirus from species C2/5 or B3, notably without affecting cell viability (Fig. 1C, D, and Supplemental Fig. 1A-F). Assaying enzymatic hydrolysis of 6-hexadecanoylamino-4-methylumbelliferyl-phosphorylcholine (HMU-PC), a fluorogenic ASMase-specific substrate demonstrated on-target action of amitriptyline and anti-ASMase siRNA (Fig. 1e). This was further corroborated by gain-of-function experiments where addition of bacterial SMase (bSMase) to ASMase-defective fibroblasts (GM00112) (Levran et al., 1992) strongly enhanced HAdV-C5_GFP infection (Fig. 1F). These results identify ASMase as an important regulator of adenovirus infection.

ASMase enhances virus endocytosis

ASMase is involved in membrane homeostasis and constitutively hydrolyses SM to ceramide and phosphorylcholine in late endosomes and lysosomes (reviewed in Beckmann et al., 2014). It controls inflammatory cytokine signaling and is implicated in hepatic pathology, cardiovascular pathophysiology and diabetes. Mutations in ASMase lead to lysosomal storage disease, for example Niemann-Pick disease types A and B (Levran et al., 1992).

To unravel the function of ceramide lipids in adenovirus infection, we investigated specific steps in virus entry. Virus attachment to cells or fiber shedding were unaffected by the ASMase inhibitor amitriptyline (Fig. 2A, B). However, ASMase inhibition delayed the kinetics of virus endocytosis in HeLa cells (Fig. 2C) or normal human WI-38 fibroblasts (not shown). Incubation of HeLa cells with bSMase rapidly increased the ceramide and reduced the SM levels without affecting the PC levels (Fig. 2D). Importantly, addition of bSMase together with the virus inoculum readily rescued the uptake of HAdV-C2 in amitriptyline-treated cells, and this effect was blunted by the soluble bSMase substrate HMU-PC (Fig. 2E). Notably, bSMase accelerated the internalization of TS1 (Fig. 2F). This underlines that SMase activity and high ceramide levels on the plasma membrane enhance HAdV endocytosis, possibly by directly affecting physical properties of the membrane. The results are in line with previous findings showing that ceramide levels correlated with increased endosomal and exosomal budding (Sandhoff, 2013; Tam et al., 2010).

Ceramide enhances protein-VI interactions with membranes

Protein-VI is the *bona fide* membrane lytic factor of adenovirus (Maier et al., 2010; Moyer et al., 2011; Wiethoff et al., 2005). It interacts with lipid bilayers *in vitro*, ruptures liposomes, and gets exposed on the incoming virus prior to membrane penetration (Burckhardt et al., 2011; Suomalainen et al., 2013).

We addressed if ceramide lipids were involved in exposing and retaining protein-VI on membranes. While inhibition of ASMase reduced membrane retention of protein-VI during virus entry, simultaneous addition of bSMase and virus to cells fully reverted this impairment, consistent with the interpretation that ceramide enhances interaction of protein-VI with membranes (Fig. 3A). This was supported by the finding that amitriptyline inhibited virus penetration to the cytosol at 15 min pi (Fig. 3B), a time point when most viruses were internalized (Supplemental Fig. 2A, B). The addition of bSMase rescued the escape of HAdV-C2, while TS1, which fails to expose protein-VI due to failure in releasing fibers and pentons (Burckhardt et al., 2011), remained trapped in the endo-lysosomal network (Fig. 3B).

We next assessed if protein-VI specifically interacted with ceramide-rich membranes. Partially uncoated viral particles were exposed to liposomes composed of either PC (1-palmitoyl-2-oleoyl-*sn*-glycero-3-phosphocholine), PC:SM 99:1 or PC:CER (ceramide) 99:1. Liposomes bound to viral proteins were separated from soluble material by floatation in a density gradient and analyzed by immunogold EM with an antibody against protein-VI (Fig. 4A-C). While protein-VI floating with PC vesicles was nearly undetectable, protein-VI strikingly associated with sphingolipid-containing membranes, with a strong preference for ceramide over SM.

To analyze how these interactions influence the integrity of liposomes, we performed liposome rupture assays (Fig. 4D). Liposomes were produced from total lipid extracts obtained from HeLa cells, and enriched in ceramide by bSMase treatment. They were loaded with self-quenching concentrations of carboxy-fluorescein. Incubation with uncoated HAdV-C5 triggered rupture of liposomes, a phenomenon that was further enhanced by ceramide. To address the role of protein-VI in this process, we tested the HAdV-C5 mutant VI-L40Q. This virus harbors a point mutation in the N-terminal amphipathic α-helix of protein-VI and exhibits attenuated membrane lysis activity (Moyer et al., 2011). VI-L40Q led to limited leakage of high-ceramide liposomes compared to HAdV-C5. This confirmed that protein-VI is the primary viral mediator of membrane rupture. We conclude that a lipid microenvironment enriched

in ceramide favors endocytosis of adenovirus, and enhances endosomal membrane rupture induced by the virus.

Plasma membrane lesion by incoming protein-VI triggers lysosomal exocytosis and enhances endosomal penetration of virus

Cells can repair membrane lesions from toxins or mechanical stress by exocytosis of lysosomal ASMase, and endocytosis of the injured membranes (Andrews et al., 2014). We tested whether ASMase was relocalized to the plasma membrane by exocytosis, and collected the supernatant of infected cells for activity tests with the lysosomal enzymes ASMase and β-hexosaminidase. We strikingly observed increased activity of both enzymes immediately after virus binding to HeLa or Wi-38 cells (Fig. 5A, B, and Supplemental Fig. 3A, B). Lysosomal exocytosis was ligand-specific, as TS1, cholera toxin B or competitive inhibition of virus binding by a soluble form of the primary virus receptor CAR (CARex-FC) did not release ASMase or β-hexosaminidase into the supernatant. Importantly, β-hexosaminidase translocation was independent of ASMase activity, since amitriptyline treatment released normal amounts of β-hexosaminidase from HAdV infected cells (Fig. 5A). Neither control nor amitriptyline treated infected cells released large amounts of the cytosolic enzyme lactate dehydrogenase, indicating that the plasma membrane was not grossly damaged by the virus (Supplemental Fig. 3A, B). Instead, HAdV-C2 inoculated cells had reduced amounts of lysotracker positive organelles at 20 min post infection (pi) compared to 0 min, or uninfected cells, suggesting lysosomal exocytosis (Supplemental Fig. 3C).

The entry of Ca^{2+} into wounded cells triggers membrane repair processes that seal off the wound within seconds (McNeil et al., 2003). We therefore tested if cytosolic Ca^{2+} was transiently increased (so called Ca^{2+} transients) during virus entry. We first noticed that secretion of β-hexosaminidase triggered by HAdV entry depended on extracellular Ca^{2+} but not Mg^{2+} (Fig. 5C). In addition, extracellular Ca^{2+} enhanced HAdV-C5_GFP expression and infection with wild type HAdV-C2 (Supplemental Fig. 3D, and Greber et al., 1997), as well as HAdV-C5 but not TS1 endocytosis (Supplemental Fig. 3E, F). These data suggest that Ca^{2+}-dependent lysosomal exocytosis supports infection. This notion was reinforced by the observation that HAdV-C5 escape from endosomes was inhibited by the microtubule depolymerizing agent nocodazole (Fig. 5D, Supplemental Fig. 3G), an inhibitor of lysosomal exocytosis and membrane sealing (Togo, 2006). Notably, inhibition of endosomal

escape of HAdV-C2 by nocodazole was bypassed by the addition of bSMase to the inoculum (Fig. 5D). This indicated that surface ASMase compensated for lack of lysosomal exocytosis in virus escape from endosomes.

We next visualized the dynamics of Ca^{2+} fluxes upon inoculation of HAdV-C2/5-Atto565 or TS1 to cells expressing the Ca^{2+} sensor GCamP5G (GCamP). The inocula contained minimal amounts of broken particles (<0.3%), as indicated by measuring protein-VI exposure on viruses attached to the cell surface at 4°C (Supplemental Fig. 4A). While resting cells rarely showed Ca^{2+} spikes, HAdV-C2 infected cells showed frequent cytosolic Ca^{2+} transients, which correlated in time with virus binding and endocytosis (Fig. 6A, Supplemental Fig. 4B and Supplemental Video 1). Note that virus endocytosis occurs within a few min after virus attachment to the cells, as indicated by bulk measurements and single virus total internal reflection microscopy (Burckhardt et al., 2011; Greber et al., 1993; Suomalainen et al., 2013). Ca^{2+} transients were not observed with TS1, or in absence of extracellular Ca^{2+} (Fig. 6B and Supplemental Data Fig. 4C, D).

We analyzed the integrity of the plasma membrane by time-lapse imaging of propidium iodide (PI), a membrane impermeable substance that becomes fluorescent upon binding to nucleic acids in the cytosol or the nucleus (Jimenez et al., 2014). Incoming HAdV-C5 provoked the influx of PI from the extracellular medium, visible as discrete spots several micrometers in diameter near the cell periphery (Fig. 6C). The PI signals lasted for a few seconds without staining the nucleus, and strictly correlated to cytosolic Ca^{2+} spikes (Fig. 6C, Supplemental Videos 2-4). The size of the HAdV-induced plasma membrane lesion is not known. But it is likely smaller than the virus, as virus did not penetrate the plasma membrane (Meier et al., 2002), and PI influx was similar to UV-laser induced plasma membrane wounds that were about 50 nm in diameter (Jimenez et al., 2014). Very similar PI fluxes were also observed in adenovirus inoculated cells expressing Dyn2K44A-GFP (Fig. 6D). Dyn2K44A-GFP blocks virus endocytosis but not initial steps of uncoating (Greber et al., 1993; Meier et al., 2002; Nakano et al., 2000). The results show that incoming virus induces small transient lesions in the plasma membrane and allows rapid membrane repair. In only rare cases, cells exhibited non-resolvable PI staining (Fig. 6E marked by *, and Supplemental Fig. 4E), indicating a failure of lesion repair. These non-resolving cells showed extensive plasma membrane blebbing, a predictor for apoptosis (Supplemental Fig. 4E, Supplemental Video 5).

We tested if protein-VI was involved in plasma membrane wounding, and measured the PI signal in cells inoculated with lysates from HAdV-C2, HAdV-C5 or the penetration impaired HAdV-C5_VI-L40Q mutant. Results show that PI influx was significantly reduced with the mutant compared to wild type virus (Fig. 6F, G). In addition, a neutralizing anti-protein-VI antibody but not control anti-protein-VIII antibody reduced PI influx into cells treated with uncoated HAdV-C2 (Fig. 6G). These observations further support the importance of protein-VI for transient plasma membrane permeabilisation, and are in accordance with reports showing a capacity of adenovirus to permeabilise the plasma membrane (Di Paolo et al., 2013; Wickham et al., 1994).

Discussion

Our data now establish a mechanistic correlation between small wounds of the plasma membrane and virus penetration through endosomal membranes, which are both mediated by protein-VI. The results indicate that protein-VI triggers a positive feedback loop involving lysosomal secretion, endocytosis and lipid modification, and thereby enhances the membrane disruption activity of the virus, and infection (Fig. 7).

Membrane ruptures are wide-spread in cell biological and immunological patho-physiology. They have drastic consequences for cell integrity but also provide opportunities for morphogenesis, for example assembly of large DNA viruses in the cytoplasm, such as poxviruses or mimivirus (Mutsafi et al., 2013; Suarez et al., 2013). Membrane rupture is a key process for many non-enveloped viruses to access the cytosol. Cues for membrane rupture involve capsid proteolysis and exposure of viral lytic factors in case of reovirus (Schulz et al., 2012; Zhang et al., 2009), or low endosomal Ca^{2+} in case of rotavirus (Abdelhakim et al., 2014). Interestingly, both viruses damage membranes and use endocytosis for infection, but how these processes are connected has remained unknown.

Virus-induced membrane rupture is a multi-step process

Using adenovirus as a model, we demonstrate a multi-step mechanism to rupture cellular membranes. The distinct steps involve highly coordinate changes in the

incoming virus and the receiving cell. Adenovirus is a medium-sized non-enveloped virus with a capsid diameter of about 90 nm (Mangel and San Martin, 2014; Nemerow et al., 2012). It is an intricate molecular machine designed to deliver a DNA genome into the host nucleus. A step-by-step entry program is facilitated by spatial and temporal cues from the cell, and allows the virus to overcome the barriers to the nucleus (Wolfrum and Greber, 2013). Initial mechanical cues from the cell surface virus receptors, the primary receptor CAR and the secondary receptor integrins, expose the membrane lytic protein-VI (Burckhardt et al., 2011). Protein-VI has an amphipathic alpha helix smaller than 50 amino acids, a large fraction of which is conserved across adenovirus types (Moyer et al., 2011; Wiethoff et al., 2005). It is akin to antimicrobial peptides that are capable of membrane permeabilization (Last et al., 2013). These peptides displace the polar lipid head groups and integrate their hydrophobic side into the hydrocarbon backbone of membranes. At a critical protein to lipid ratio, these peptides either traverse the lipid bilayer or form stable pores, thereby causing membrane damage (Shai, 1999).

Although the virus contains more than 300 copies of protein-VI, initial membrane lesions are small and may comprise only a few copies of protein-VI. Based on analogy with laser-induced plasma membrane lesions (Jimenez et al., 2014), we estimate that these initial lesions are too small for the virus to pass through. But these small wounds are conducive to Ca^{2+} signaling, and this induces lysosomal exocytosis and thus increases ceramide lipid species at the plasma membrane leading to enhancement of virus endocytosis. The ability of protein-VI to bind ceramide-rich membranes finally destabilizes and ruptures the endosomal membrane enclosing the virus. Based on the earlier observation that cytosolic virus is free of protein-VI (Burckhardt et al., 2011), we speculate that endosomal cues (other than low pH) facilitate the release of additional protein-VI from the interior of the virus, and further enhance endosomal rupture.

We consider it unfavorable for the virus to penetrate the plasma membrane, because cells respond to and counteract plasma membrane stress by increasing cytoskeletal tension in the cortex, exocytosis or regulation of ion flux (Groulx et al., 2006). Rather than penetrating the plasma membrane, the virus is engulfed into leaky endosomes, and penetrates endosomal membranes that are low in stress-compensatory activities. Endosomal membrane stress is further enhanced by protein-VI, which perturbs membranes by forming positive curvature (Maier et al., 2010). Such lipid-protein interactions may represent a conserved mechanism of membrane

destabilization that is also used by bacterial membrane-lytic proteins. For example, *Listeria monocytogenes* uses a pore-forming toxin to induce endocytosis and escape from host cell vacuoles (Vadia et al., 2011). Membrane disruption may involve alterations of intrinsic lipid fluctuation frequencies leading to dose-dependent membrane rupture (Last et al., 2013). Tuning of the membrane lytic activity of protein-VI by involving lysosomal exocytosis, ASMase and ceramide lipids ensures that the insults to cell integrity remain localized and do not lead to massive cell damage. This is a key for cell survival, and ensuing steps of infection.

ASMase and sphingolipids are key elements for infectious disease

Ceramide is derived from SM by ASMase and supports adenovirus membrane penetration. SM is highly abundant in the outer leaflet of the plasma membrane, traffics through the endo-lysosomal network, and plays an essential role in the formation of lipid rafts ((for a review, see Simons and Toomre, 2000)). SM-enriched membrane domains mediate the binding of Ebolavirus to cells, or facilitate early steps in measles virus infection of immature dendritic cells (Beckmann et al., 2014; Schneider-Schaulies and Schneider-Schaulies, 2014). Ceramide-enriched membrane domains are sites of increased viral and bacterial pathogen uptake owing to curvature induction and signaling (Beckmann et al., 2014; Simonis et al., 2014). ASMase is a clinically important lysosomal enzyme, and an early responder in inflammatory cytokine signaling in cardiovascular patho-physiological conditions and diabetes, which is, for example, associated with Coxsackie virus infection of beta-cells of the pancreas. An inhibitor of ASMase, amitriptyline, which we found inhibits adenovirus infection, is used to block bacterial infections in CFTR patients (Becker et al., 2010; Nahrlich et al., 2013; Teichgraber et al., 2008). In addition ASMase supports Japanese encephalitis virus and human rhinovirus infections, although it is not clear if this involves lysosomal exocytosis (Grassme et al., 2005; Miller et al., 2012; Tani et al., 2010).

Lysosomal exocytosis and endocytosis are associated with repair of virus-induced membrane damage

Lysosomal exocytosis is a general response of cells to plasma membrane wounding, and is associated with membrane repair (Andrews et al., 2014). Restoring membrane integrity is crucial to preclude necrosis and apoptosis, and reduce inflammation from necrotic cells. Lysosomal exocytosis is robustly induced by small wounds from the

incoming adenoviruses of both species B and C, but exactly how the wounds in the membrane are repaired is not yet known. Although plasma membrane blebbing and shedding of micro-vesicles have been implicated in repair of laser induced membrane lesions through the AAA-ATPase VPS4 (Jimenez et al., 2014), we found no indication for involvement of VPS4 in HAdV-C5_GFP entry or membrane shedding (data not shown). We therefore consider this process unlikely to account for wound repair in adenovirus infected cells. Instead, it is more likely that the repair mechanism involves lysosomal exocytosis followed by endocytosis of damaged membranes. As shown in this study, lysosomal exocytosis delivers ASMase outside of the cell, increases cellular ceramide levels and enhances the rate of viral endocytosis. Viral endocytosis is cholesterol and dynamin-dependent (Imelli et al., 2004; Meier et al., 2002), and might thereby help to remove damaged membrane areas, akin to cholesterol-dependent endocytosis which removes wounds caused by bacterial toxins (Idone et al., 2008). We can, however, not exclude that other endocytic processes are involved in clearing protein-VI induced membrane damage. Noticeably, adenoviruses induce dynamin-independent cholesterol-dependent macropinocytosis with features of membrane ruffling, blebbing and wobbling (Amstutz et al., 2008; Fleischli et al., 2005; Kalin et al., 2010; Meier et al., 2002; Nagel et al., 2003). Macropinocytosis requires CAR, integrin or CD46 receptors, as well as cortical actin dynamics induced by Ca^{2+} transients. This is similar to the endocytic pathway clearing streptolysin O induced membrane damage (Corrotte et al., 2012; Idone et al., 2008).

Experimental Procedures

Lipid extraction and mass spectrometry

For lipid profiling, 8 x 10^6 HeLa cells were infected for 30 min with 6.8-ml inocula containing 2 µg of HAdV-C2 or TS1. Total lipid extracts were collected according to a modified Bligh and Dyer protocol and 159 lipid species were analyzed by HPLC MS/MS as described in (Tanner et al., 2014). The values listed in Supplemental Data Tab. 1 represent the molar fraction of each lipid species compared to the total amount of measured lipids. The $\log_2$ fold change of lipid abundance at 0 and 30 min pi was plotted, and statistical significance was evaluated by unpaired Student t-test (two-tailed, $p<0.05$). The experimental variance is indicated in the y-axis (p-value). For ceramide quantification in bSMase treated samples, 2 x 10^6 HeLa cells were incubated for 5 min with 0.2 U bacterial sphingomyelinase from *S. aureus* (bSMase; Sigma). Total lipid extracts were collected as previously described (Guan and Wenk, 2012), except that cell suspensions in chloroform:methanol (1:2) were vortexed 1 min and incubated on ice for 4 min, three times. After adding 300 µl chloroform and 200 µl ultra pure H_20 samples were vortexed for 1 min and incubated on ice for 1 min, three times. Ceramide and sphingomyelin were quantified using LC-MS (Guan et al., 2013).

Infection assays

Cells grown on 96-well imaging plates (Greiner Bio-one) were infected in DMEM-0.2% FAF-BSA fraction V (Roche) for 16-24 h to reach an infection level of 20-40%. Cells were fixed, stained with DAPI, anti-VI (Burckhardt et al., 2011) or anti-hexon (mab 8052, Millipore), and imaged by automated fluorescence microscopy with ImageXpress Micro (Molecular Devices). Mean fluorescence intensity of the nuclear GFP signal and percentage of either GFP expressing or protein-VI stained cells was evaluated using a custom programmed Matlab routine (Matlab R2009b, available upon request). For drug interference, cells were treated with 50 µM myriocin (He et al., 2004) (Enzo Life Sciences), 100 µM fumonisin B1 (Wang et al., 1991) (Tocris), 50 µM GW4869 (Luberto et al., 2002), 25 µM amitriptyline or 5 µM fluoxetine (Kornhuber et al., 2008) (all Sigma) for 4 h before and during infection with either HAdV-C5_GFP, HAdV-C2 or HAdV-B3. For siRNA mediated knockdown of ASMase, HeLa cells were

subjected to reverse-transfection with 10 nM siRNA using lipofectamine RNAiMAX (LifeTechnologies) and cells were infected after 72 h. ON-TARGET *Plus* siRNA sequences against human SMPD1 (J006676-05; J-006676-06) and non-targeting sequences were obtained from Thermo Scientific Dharmacon; siRNA against GFP from Mycrosynth. For rescue experiments in GM00112 cells, inocula were supplemented with 0.024 U/ml of bacterial sphingomyelinase (bSMase) from *S. aureus* (Sigma). For Ca^{2+}-free infection assays, cells were exposed to the inoculum with or without Ca^{2+} for 2 h, then placed for further 14 h into DMEM-0.2% FAF-BSA to avoid cell detachment.

Detection of cytosolic viruses

Cytosolic viruses were distinguished from endosomal viruses using SLO-penetration assay and EM analysis. Both procedures were performed exactly as described in (Suomalainen et al., 2013). Briefly, cells were pre-treated with 25 µm amitriptyline for 4 h, 10 µM nocodazole for 1 h, or left untreated and exposed to a cold-synchronised infection for various times. For SLO-assay, streptolysin O (SLO; Sigma) was used to selectively permeabilize plasma membranes and allow perfusion of antibodies to the cytosol but not to the lumen of intracellular organelles. HAdV-C2-Alexa488 and TS1-Alexa488 were immuno-stained with rabbit anti-Alexa Fluor 488 antibodies at 4°C for 1 h (Life Technologies). Samples were processed as described in the previous section. Mean signal intensities of anti-Alexa Fluor 488 staining associated to viruses per cell are indicated. For quantification of EM sections, the number of viruses at the plasma membrane, in endosomes and in the cytosol was determined by manual counting.

Liposome floatation

1-palmitoyl-2-oleoylphosphatidylcholine (PC), N-octadecanoyl-D-*erythro*-sphingosine (CER), N-octadecanoyl-D-*erythro*-sphingosylphosphorylcholine (SM) and extruder were obtained from Avanti Polar Lipids. Dried lipid films composed of PC, PC:CER 99:1 mol % and PC:SM 99:1 mol % were hydrated in liposome buffer (10 mM HEPES, 150 mM NaCl, 2 mM $CaCl_2$, pH 7.5) at 1 mg/ml. Lipid suspensions were subjected to 20 freeze-thaw cycles and extruded 11 times through a 100 nm

polycarbonate-membrane. Viruses were pre-incubated at 45°C for 10 min to induce uncoating (Wiethoff et al., 2005). Uncoated viruses (4 μg) were incubated with liposomes (100 μg) at 37°C for 15 min, samples mixed with Optiprep (Sigma) to a final concentration of 15%. Each 600 µl sample was overlaid with a density gradient of Optiprep (1.5 ml of 10%, 1 ml of 2.5% and 0% in liposomes buffer) and centrifuged at 100'000 x *g* at 4°C for 2 h. Low density, empty liposomes floated to the top fraction of the gradient, while liposomes bound to viral proteins concentrated into a lower band. Fractions of 400 µl were collected, subjected to immuno-gold labeling with anti-VI antibodies and analyzed by EM negative staining with uranyl acetate. Images were blindly acquired at 25'000 x magnification without detecting the gold signal. Each image was magnified up to 80'000, and the total number of liposomes and liposomes bound to gold were counted. To avoid underestimation of binding, when one liposome bound to n+1 gold, n liposomes with 100% binding (meaning one liposome bound to one VI-gold) were included in the statistics.

Liposome leakage

Total lipid extracts of 5 x 10^6 HeLa cells were prepared as described (Tanner et al., 2014), dried and re-hydrated in 0.2 M 6-carboxyfluorescein (6-CF; Sigma). Liposomes were produced as described for the liposome-binding assay. To remove unincorporated 6-CF, the sample was passed through a gravity flow column (1 ml, Biorad) filled with Sephadex-G50 (Pharmacia Biotech; hydrated overnight at 4°C) was centrifuged at 2'000 x *g* for 2 min. One hundred μl liposomes were loaded on the gel and centrifuged at 2'000 x *g* for 2 min. The eluate was cleared by a second step of centrifugation on a new column and the final volume brought to 200 μl with liposome buffer. Cleared liposomes from approximately 5 x 10^4 cells were immediately pre-incubated with 0.48 U/ml bSMase or liposome buffer for 15 min, and further incubated with 5 μg/ml uncoated HAdV-C5-GFP or 5 μg/ml uncoated VI-L40Q virus at 37°C for 15 min. One hundred % of liposome leakage was determined by adding Triton X-100 to a final concentration of 0.5 %. Fluorescence was measured with M200 Infinite Plate Reader (Tecan) at 485 nm excitation/530 nm emission. The percentage of leakage was calculated using the formula: 100 -[(*F*meas _ *F*0)/(*F*tx100 _ *F*0)], where *F*meas is the maximum fluorescence intensity measured, *F*0 is fluorescence intensity before adding viral proteins, and *F*tx100 the fluorescence intensity in the presence of 0.5% Triton X-100, as described in (Moyer et al., 2011).

Live imaging of Ca^{2+} and propidium iodide

HeLa cells were transfected with pCMV_GCamP5G (Addgene) (Akerboom et al., 2012), and grown in 96-well imaging plates (Greiner Bio-one) for 24 h. Cells exposed to 1-10 μg/ml HAdV-C2-Atto565 or 1-10 μg/ml HAdV-C2 in presence of 0.2 mg/ml propidium iodide (Molecular Probes) or absence of Ca^{2+} were imaged for 0 to 15 min at 37°C with a Leica SP5 confocal microscope equipped with 40 × (oil immersion, numerical aperture 1.25) objective. Z-stacks composed of 4 x 0.5 µm steps were recorded at a frequency of 8000 Hz applying bidirectional scan, line averaging 32x and minimized acquisition time. Total fluorescence intensity per cell or per area was quantified with MacBiophotonics ImageJ (McMaster University). Quantifications show a minimum of 16 representative cells out of the 50 to 200 cells imaged in at least 3 movies per condition.

Statistical analysis

Statistical analyses were performed using GraphPad Prism software (Version 5, GraphPad Software, Inc. La Jolla). Population data are plotted as bars or symbols and single-cell-based assays represented as scatter dot plots, where the horizontal bars indicate the mean value and the vertical bars the standard error of the mean. Two-tailed P-values were calculated by unpaired t-test with confidence interval 95%. Other methods are described in detail in Supplemental Procedures, including flow cytometry, lysotracker quantifications, ASMase activity and cell toxicity assays, or enzymatic assays for ASMase and lactate dehydrogenase activities.

Authors contributions

Conceived, performed or interpreted experiments (SL, MS, KB, LT, MW, XG, MG, UC, UFG), wrote manuscript (SL, UFG), conceived and coordinated study (UFG).

Acknowledgements

We thank Artur Yakimovich for support in image analyses, Silvio Hemmi for anti-CAR antibody and CARex-FC fusion protein, the Center for Microscopy and Image Analyses of UZH for their support in fluorescence microscopy, and the members of the Greber lab for valuable discussions.

Funding

Funding was obtained from the Swiss National Science Foundation (31003A_141222/1 to UFG, PZ00P3_136738-1 to XLG), the Research and Technology Development project LipidX from SystemsX.ch (LipidX-2008/011 to UFG and MRW), and the German Federal Ministry of Education and Research grant to the German Center for Diabetes Research (DZD e.V.) (M.G. and Ü.C.).

References

Abdelhakim, A.H., Salgado, E.N., Fu, X., Pasham, M., Nicastro, D., Kirchhausen, T., and Harrison, S.C. (2014). Structural correlates of rotavirus cell entry. PLoS Pathog *10*, e1004355.

Akerboom, J., Chen, T.W., Wardill, T.J., Tian, L., Marvin, J.S., Mutlu, S., Calderón, N.C., Esposti, F., Borghuis, B.G., Sun, X.R.*, et al.* (2012). Optimization of a GCaMP calcium indicator for neural activity imaging. J Neurosci *32*, 13819-13840.

Altschuler, Y., Barbas, S.M., Terlecky, L.J., Tang, K., Hardy, S., Mostov, K.E., and Schmid, S.L. (1998). Redundant and distinct functions for dynamin-1 and dynamin-2 isoforms. J Cell Biol *143*, 1871-1881.

Amstutz, B., Gastaldelli, M., Kälin, S., Imelli, N., Boucke, K., Wandeler, E., Mercer, J., Hemmi, S., and Greber, U.F. (2008). Subversion of CtBP1 controlled macropinocytosis by human Adenovirus serotype 3. EMBO J *27*, 956-966.

Andrews, N.W., Almeida, P.E., and Corrotte, M. (2014). Damage control: cellular mechanisms of plasma membrane repair. Trends Cell Biol *24*, 734-742.

Becker, K.A., Riethmuller, J., Luth, A., Doring, G., Kleuser, B., and Gulbins, E. (2010). Acid sphingomyelinase inhibitors normalize pulmonary ceramide and inflammation in cystic fibrosis. Am J Respir Cell Mol Biol *42*, 716-724.

Beckmann, N., Sharma, D., Gulbins, E., Becker, K.A., and Edelmann, B. (2014). Inhibition of acid sphingomyelinase by tricyclic antidepressants and analogons. Front Physiol *5*, 331.

Bi, G.Q., Alderton, J.M., and Steinhardt, R.A. (1995). Calcium-regulated exocytosis is required for cell membrane resealing. J Cell Biol *131*, 1747-1758.

Browning, C., Shneider, M.M., Bowman, V.D., Schwarzer, D., and Leiman, P.G. (2012). Phage pierces the host cell membrane with the iron-loaded spike. Structure *20*, 326-339.

Burckhardt, C.J., Suomalainen, M., Schoenenberger, P., Boucke, K., Hemmi, S., and Greber, U.F. (2011). Drifting motions of the adenovirus receptor CAR and immobile integrins initiate virus uncoating and membrane lytic protein exposure. Cell Host Microbe *10*, 105-117.

Corrotte, M., Fernandes, M.C., Tam, C., and Andrews, N.W. (2012). Toxin pores endocytosed during plasma membrane repair traffic into the lumen of MVBs for degradation. Traffic *13*, 483-494.

Cossart, P., and Helenius, A. (2014). Endocytosis of viruses and bacteria. Cold Spring Harb Perspect Biol *6*.

Di Paolo, N.C., Doronin, K., Baldwin, L.K., Papayannopoulou, T., and Shayakhmetov, D.M. (2013). The transcription factor IRF3 triggers "defensive suicide" necrosis in response to viral and bacterial pathogens. Cell reports *3*, 1840-1846.

Ebbinghaus, C., Al-Jaibaji, A., Operschall, E., Schoeffel, A., Peter, I., Greber, U.F., and Hemmi, S. (2001). Functional and selective targeting of adenovirus to high

affinity Fcg receptor I positive cells using a bispecific hybrid adaptor. J Virol *75*, 480-489.

Ewer, K.J., O'Hara, G.A., Duncan, C.J., Collins, K.A., Sheehy, S.H., Reyes-Sandoval, A., Goodman, A.L., Edwards, N.J., Elias, S.C., Halstead, F.D.*, et al.* (2013). Protective CD8+ T-cell immunity to human malaria induced by chimpanzee adenovirus-MVA immunisation. Nat Commun *4*, 2836.

Fleischli, C., Verhaagh, S., Havenga, M., Sirena, D., Schaffner, W., Cattaneo, R., Greber, U.F., and Hemmi, S. (2005). The Distal Short Consensus Repeats 1 and 2 of the Membrane Cofactor Protein CD46 and Their Distance from the Cell Membrane Determine Productive Entry of Species B Adenovirus Serotype 35. J Virol *79*, 10013-10022.

Ganzenmueller, T., Buchholz, S., Harste, G., Dammann, E., Trenschel, R., and Heim, A. (2011). High lethality of human adenovirus disease in adult allogeneic stem cell transplant recipients with high adenoviral blood load. J Clin Virol *52*, 55-59.

Gastaldelli, M., Imelli, N., Boucke, K., Amstutz, B., Meier, O., and Greber, U.F. (2008). Infectious adenovirus type 2 transport through early but not late endosomes. Traffic *9*, 2265-2278.

Gault, C.R., Obeid, L.M., and Hannun, Y.A. (2010). An overview of sphingolipid metabolism: from synthesis to breakdown. Adv Exp Med Biol *688*, 1-23.

Grassme, H., Riehle, A., Wilker, B., and Gulbins, E. (2005). Rhinoviruses infect human epithelial cells via ceramide-enriched membrane platforms. J Biol Chem *280*, 26256-26262.

Greber, U.F., Suomalainen, M., Stidwill, R.P., Boucke, K., Ebersold, M., and Helenius, A. (1997). The role of the nuclear pore complex in adenovirus DNA entry. EMBO J *16*, 5998-6007.

Greber, U.F., Webster, P., Weber, J., and Helenius, A. (1996). The role of the adenovirus protease on virus entry into cells. EMBO J *15*, 1766-1777.

Greber, U.F., Willetts, M., Webster, P., and Helenius, A. (1993). Stepwise dismantling of adenovirus 2 during entry into cells. Cell *75*, 477-486.

Groulx, N., Boudreault, F., Orlov, S.N., and Grygorczyk, R. (2006). Membrane reserves and hypotonic cell swelling. The Journal of membrane biology *214*, 43-56.

Guan, X.L., Cestra, G., Shui, G., Kuhrs, A., Schittenhelm, R.B., Hafen, E., van der Goot, F.G., Robinett, C.C., Gatti, M., Gonzalez-Gaitan, M.*, et al.* (2013). Biochemical membrane lipidomics during Drosophila development. Dev Cell *24*, 98-111.

Guan, X.L., and Wenk, M.R. (2012). Targeted and non-targeted analysis of membrane lipids using mass spectrometry. Methods Cell Biol *108*, 149-172.

He, Q., Johnson, V.J., Osuchowski, M.F., and Sharma, R.P. (2004). Inhibition of serine palmitoyltransferase by myriocin, a natural mycotoxin, causes induction of c-myc in mouse liver. Mycopathologia *157*, 339-347.

Hendrickx, R., Stichling, N., Koelen, J., Kuryk, L., Lipiec, A., and Greber, U.F. (2014). Innate Immunity to Adenovirus. Hum Gene Ther *25*, 265–284.

Idone, V., Tam, C., Goss, J.W., Toomre, D., Pypaert, M., and Andrews, N.W. (2008). Repair of injured plasma membrane by rapid Ca2+-dependent endocytosis. J Cell Biol *180*, 905-914.

Imelli, N., Meier, O., Boucke, K., Hemmi, S., and Greber, U.F. (2004). Cholesterol is required for endocytosis and endosomal escape of adenovirus type 2. J Virol *78*, 3089-3098.

Jimenez, A.J., Maiuri, P., Lafaurie-Janvore, J., Divoux, S., Piel, M., and Perez, F. (2014). ESCRT machinery is required for plasma membrane repair. Science *343*, 1247136.

Kalin, S., Amstutz, B., Gastaldelli, M., Wolfrum, N., Boucke, K., Havenga, M., DiGennaro, F., Liska, N., Hemmi, S., and Greber, U.F. (2010). Macropinocytotic uptake and infection of human epithelial cells with species B2 adenovirus type 35. J Virol *84*, 5336-5350.

Keefe, D., Shi, L., Feske, S., Massol, R., Navarro, F., Kirchhausen, T., and Lieberman, J. (2005). Perforin triggers a plasma membrane-repair response that facilitates CTL induction of apoptosis. Immunity *23*, 249-262.

Kornhuber, J., Tripal, P., Reichel, M., Terfloth, L., Bleich, S., Wiltfang, J., and Gulbins, E. (2008). Identification of new functional inhibitors of acid

sphingomyelinase using a structure-property-activity relation model. J Med Chem *51*, 219-237.

Last, N.B., Schlamadinger, D.E., and Miranker, A.D. (2013). A common landscape for membrane-active peptides. Protein Sci *22*, 870-882.

Levran, O., Desnick, R.J., and Schuchman, E.H. (1992). Identification and expression of a common missense mutation (L302P) in the acid sphingomyelinase gene of Ashkenazi Jewish type A Niemann-Pick disease patients. Blood *80*, 2081-2087.

Luberto, C., Hassler, D.F., Signorelli, P., Okamoto, Y., Sawai, H., Boros, E., Hazen-Martin, D.J., Obeid, L.M., Hannun, Y.A., and Smith, G.K. (2002). Inhibition of tumor necrosis factor-induced cell death in MCF7 by a novel inhibitor of neutral sphingomyelinase. J Biol Chem *277*, 41128-41139.

Maier, O., Galan, D.L., Wodrich, H., and Wiethoff, C.M. (2010). An N-terminal domain of adenovirus protein VI fragments membranes by inducing positive membrane curvature. Virology *402* 11-19.

Mangel, W.F., and San Martin, C. (2014). Structure, Function and Dynamics in Adenovirus Maturation. Viruses *6*, 4536-4570.

Matthes-Martin, S., Boztug, H., and Lion, T. (2013). Diagnosis and treatment of adenovirus infection in immunocompromised patients. Expert Rev Anti Infect Ther *11*, 1017-1028.

McNeil, P.L., Miyake, K., and Vogel, S.S. (2003). The endomembrane requirement for cell surface repair. Proc Natl Acad Sci U S A *100*, 4592-4597.

Meier, O., Boucke, K., Hammer, S.V., Keller, S., Stidwill, R.P., Hemmi, S., and Greber, U.F. (2002). Adenovirus triggers macropinocytosis and endosomal leakage together with its clathrin-mediated uptake. J Cell Biol *158*, 1119-1131.

Miller, M.E., Adhikary, S., Kolokoltsov, A.A., and Davey, R.A. (2012). Ebolavirus requires acid sphingomyelinase activity and plasma membrane sphingomyelin for infection. J Virol *86*, 7473-7483.

Moyer, C.L., Wiethoff, C.M., Maier, O., Smith, J.G., and Nemerow, G.R. (2011). Functional genetic and biophysical analyses of membrane disruption by human adenovirus. J Virol *85*, 2631-2641.

Mutsafi, Y., Shimoni, E., Shimon, A., and Minsky, A. (2013). Membrane assembly during the infection cycle of the giant Mimivirus. PLoS Pathog *9*, e1003367.

Nagel, H., Maag, S., Tassis, A., Nestle, F.O., Greber, U.F., and Hemmi, S. (2003). The alphavbeta5 integrin of hematopoietic and nonhematopoietic cells is a transduction receptor of RGD-4C fiber-modified adenoviruses. Gene Ther *10*, 1643-1653.

Nahrlich, L., Mainz, J.G., Adams, C., Engel, C., Herrmann, G., Icheva, V., Lauer, J., Deppisch, C., Wirth, A., Unger, K.*, et al.* (2013). Therapy of CF-patients with amitriptyline and placebo--a randomised, double-blind, placebo-controlled phase IIb multicenter, cohort-study. Cellular physiology and biochemistry : international journal of experimental cellular physiology, biochemistry, and pharmacology *31*, 505-512.

Nakano, M.Y., Boucke, K., Suomalainen, M., Stidwill, R.P., and Greber, U.F. (2000). The first step of adenovirus type 2 disassembly occurs at the cell surface, independently of endocytosis and escape to the cytosol. J Virol *74*, 7085-7095.

Nemerow, G.R., Stewart, P.L., and Reddy, V.S. (2012). Structure of human adenovirus. Current opinion in virology *2*, 115-121.

Reddy, A., Caler, E.V., and Andrews, N.W. (2001). Plasma membrane repair is mediated by Ca(2+)-regulated exocytosis of lysosomes. Cell *106*, 157-169.

Sandhoff, K. (2013). Metabolic and cellular bases of sphingolipidoses. Biochem Soc Trans *41*, 1562-1568.

Schelhaas, M., Shah, B., Holzer, M., Blattmann, P., Kuhling, L., Day, P.M., Schiller, J.T., and Helenius, A. (2012). Entry of human papillomavirus type 16 by actin-dependent, clathrin- and lipid raft-independent endocytosis. PLoS Pathog *8*, e1002657.

Schneider-Schaulies, J., and Schneider-Schaulies, S. (2014). Sphingolipids in viral infection. Biological chemistry.

Schulz, W.L., Haj, A.K., and Schiff, L.A. (2012). Reovirus uses multiple endocytic pathways for cell entry. J Virol *86*, 12665-12675.

Settembre, C., and Ballabio, A. (2014). Lysosome: regulator of lipid degradation pathways. Trends Cell Biol.

Shai, Y. (1999). Mechanism of the binding, insertion and destabilization of phospholipid bilayer membranes by alpha-helical antimicrobial and cell non-selective membrane-lytic peptides. Biochim Biophys Acta *1462*, 55-70.

Simonis, A., Hebling, S., Gulbins, E., Schneider-Schaulies, S., and Schubert-Unkmeir, A. (2014). Differential Activation of Acid Sphingomyelinase and Ceramide Release Determines Invasiveness of Neisseria meningitidis into Brain Endothelial Cells. PLoS Pathog *10*, e1004160.

Simons, K., and Toomre, D. (2000). Lipid rafts and signal transduction. Nat Rev Mol Cell Biol *1*, 31-39.

Suarez, C., Welsch, S., Chlanda, P., Hagen, W., Hoppe, S., Kolovou, A., Pagnier, I., Raoult, D., and Krijnse Locker, J. (2013). Open membranes are the precursors for assembly of large DNA viruses. Cell Microbiol *15*, 1883-1895.

Suomalainen, M., and Greber, U.F. (2013). Uncoating of non-enveloped viruses. Current opinion in virology *3*, 27-33.

Suomalainen, M., Luisoni, S., Boucke, K., Bianchi, S., Engel, D.A., and Greber, U.F. (2013). A direct and versatile assay measuring membrane penetration of adenovirus in single cells. J Virol *87*, 12367-12379.

Tam, C., Idone, V., Devlin, C., Fernandes, M.C., Flannery, A., He, X., Schuchman, E., Tabas, I., and Andrews, N.W. (2010). Exocytosis of acid sphingomyelinase by wounded cells promotes endocytosis and plasma membrane repair. J Cell Biol *189*, 1027-1038.

Tani, H., Shiokawa, M., Kaname, Y., Kambara, H., Mori, Y., Abe, T., Moriishi, K., and Matsuura, Y. (2010). Involvement of ceramide in the propagation of Japanese encephalitis virus. J Virol *84*, 2798-2807.

Tanner, L.B., Chng, C., Guan, X.L., Lei, Z., Rozen, S.G., and Wenk, M.R. (2014). Lipidomics identifies a requirement for peroxisomal function during influenza virus replication. J Lipid Res *55*, 1357-1365.

Teichgraber, V., Ulrich, M., Endlich, N., Riethmuller, J., Wilker, B., De Oliveira-Munding, C.C., van Heeckeren, A.M., Barr, M.L., von Kurthy, G., Schmid, K.W.*, et al.*

(2008). Ceramide accumulation mediates inflammation, cell death and infection susceptibility in cystic fibrosis. Nat Med *14*, 382-391.

Togo, T. (2006). Disruption of the plasma membrane stimulates rearrangement of microtubules and lipid traffic toward the wound site. J Cell Sci *119*, 2780-2786.

Vadia, S., Arnett, E., Haghighat, A.C., Wilson-Kubalek, E.M., Tweten, R.K., and Seveau, S. (2011). The pore-forming toxin listeriolysin O mediates a novel entry pathway of L. monocytogenes into human hepatocytes. PLoS Pathog *7*, e1002356.

Walev, I., Bhakdi, S.C., Hofmann, F., Djonder, N., Valeva, A., Aktories, K., and Bhakdi, S. (2001). Delivery of proteins into living cells by reversible membrane permeabilization with streptolysin-O. Proc Natl Acad Sci U S A *98*, 3185-3190.

Wang, E., Norred, W.P., Bacon, C.W., Riley, R.T., and Merrill, A.H. (1991). Inhibition of sphingolipid biosynthesis by fumonisins. Implications for diseases associated with Fusarium moniliforme. J Biol Chem *266*, 14486-14490.

Wickham, T.J., Filardo, E.J., Cheresh, D.A., and Nemerow, G.R. (1994). Integrin avb5 selectively promotes adenovirus mediated cell membrane permeabilization. J Cell Biol *127*, 257-264.

Wiethoff, C.M., Wodrich, H., Gerace, L., and Nemerow, G.R. (2005). Adenovirus protein VI mediates membrane disruption following capsid disassembly. J Virol *79*, 1992-2000.

Wodrich, H., Henaff, D., Jammart, B., Segura-Morales, C., Seelmeir, S., Coux, O., Ruzsics, Z., Wiethoff, C.M., and Kremer, E.J. (2010). A capsid-encoded PPxY-motif facilitates adenovirus entry. PLoS Pathog *6*, e1000808.

Wolfrum, N., and Greber, U.F. (2013). Adenovirus signalling in entry. Cell Microbiol *15*, 53-62.

Zeng, X., and Carlin, C.R. (2013). Host cell autophagy modulates early stages of adenovirus infections in airway epithelial cells. J Virol *87*, 2307-2319.

Zhang, L., Agosto, M.A., Ivanovic, T., King, D.S., Nibert, M.L., and Harrison, S.C. (2009). Requirements for the formation of membrane pores by the reovirus myristoylated micro1N peptide. J Virol *83*, 7004-7014.

Figure Legends

Fig. 1: Ceramides derived from ASMase activity are enriched in adenovirus inoculated cells during entry and support infection (see also Suppl. Fig. 1, and Suppl. Tab. 1)

A) Lipidomic analysis of HeLa cells infected with HAdV-C2 or TS1 for 30 min in comparison to mock infected cells. Ceramide species are highlighted in red (increased) and blue (decreased).

B) Schematic representation of ceramide generating pathways and respective inhibitors.

C, D, E) Chemical inhibition and silencing of ASMase reduce infection and ASMase activity. HeLa cells were treated with the indicated drugs for 4 h before and 16 h during infection or transfected using lipofectamine (Lipo) with siRNA sequences specific for ASMase (siASM1, siASM2), GFP (siGFP), or non-targeted sequences (siNT) for 72 h before infection. Lysates of treated cells were incubated with HMU-PC, a fluorogenic substrate of ASMase.

F) Gain of infection by addition of bSMase to ASMase deficient GM00112 cells together with the inoculum.

Fig. 2: ASMase inhibition does not affect binding and fiber shedding, but delays virus endocytosis (see also Suppl. Fig. 2)

A) The levels of CAR and HAdV-C2 binding to HeLa cells are not affected by amitriptyline. Non-permeabilized cells treated with amitriptyline (25 µM) for 4 h were either stained for surface CAR with an antibody as described (Ebbinghaus et al., 2001), or exposed to HAdVC2-Atto488 at 4°C for 1 h followed by washing and flow cytometry analysis.

B) Fiber release in a cold-synchronized infection is not affected by amitriptyline (25 µM). Fixed cells were stained with anti-fiber antibody R72 (Greber et al., 1993), and processed for confocal microscopy. The intensity of the antibody staining colocalizing with the viruses was determined in a single cell, single virus analysis. One dot represents the average intensity of the fiber staining on viruses per cell.

C) Amitriptyline (25 µM) delays virus endocytosis. Time course analysis of endocytosis in cold-synchronized infection of HeLa cells with HAdV5-Atto565. Surface viruses were recognized by incubation with the 9C12 anti-hexon antibody at 4°C on unfixed, unpermeabilized cells. Particles positive for Atto565 but negative for 9C12 staining were considered endocytosed (Suomalainen et al., 2013). Endocytosed particles per cell were determined by confocal microscopy and Matlab software scripts.

D) Rapid increase of total ceramide and reduction of total SM upon addition of bSMase to HeLa cells without affecting the PC levels.

E, F) bSMase accelerates endocytosis of HAdV-C5-Atto565 in amitriptyline inhibited cells, and TS1-Alexa488 in untreated cells. Endocytosis was measured as described in panel c. Cells were treated with amitriptyline or untreated, and exposed to HAdV-C5-Atto565 at 4°C. Yellow shows surface particles, positive for Atto565 and 9C12 staining. Warm medium supplemented with amitriptyline, bSMase (0.012 U/ml) or bSMase mixed with a 150-fold excess of the substrate HMU-PC was added to cells at 37°C for 5 min. Endocytosis of TS1 was evaluated at 10 min post warming.

Fig. 3: Ceramide enhances capsid protein-VI binding to liposomes, membrane rupture through protein-VI, and boosts endosomal escape of virus

A) ASMase inhibition reduced VI retention on cells. Cells were pre-treated with either DMEM-0.2% fatty-acid-free bovine serum albumin (FAF-BSA) or 25 µM Ami for 4 h, incubated with HAdV-C5-Atto565 in the cold, and warmed at 37°C in medium supplemented either with Ami, 0.012 U/ml bSMase or bSMase mixed with a 150-fold excess of its *in vitro* substrate HMU-PC for 5 min. Surface viruses were recognized by incubation with the 9C12 anti-hexon antibody in unfixed, non-permeabilized cells at 4°C. Viruses positive for Atto565 but negative for 9C12 staining were scored as internalized, and VI exposure on internalized particles was evaluated. Yellow shows colocalisation between Atto565 viruses and VI staining.

B) ASMase inhibition reduced endosomal escape of HAdV-C2-Alexa488 but not that of TS1-Alexa488. Infection was performed as described above, and cytosolic viruses

scored by SLO permeabilization of the plasma membrane and perfusion of anti-Alexa488 antibodies as described (Suomalainen et al., 2013).

Fig. 4: Ceramide enhances binding to and lysis of liposomes

A) Schematic representation of a protein-VI binding assay to liposomes. Top fractions were subjected to immunogold labeling of VI and EM analyses.

B) Protein-VI exposure on heat treated viruses mimicks uncoating, as verified by immunogold labeling of VI and EM analysis.

C) Protein-VI preferentially binds to liposomes containing ceramide, as shown by EM analyses and quantification of % positive liposomes (a minimum of 250 liposomes were analyzed per condition).

D) Protein-VI-mediated leakage is enhanced in ceramide-rich liposomes. Schematic representation of a liposome leakage assay. 6-carboxyfluorescein entrapped liposomes were exposed to bSMase or left untreated. Liposomes were further incubated with uncoated HAdV-C5-GFP or uncoated VI-L40Q. 100% liposome leakage was induced by membrane solubilization with Triton X-100.

Fig. 5: Incoming adenovirus triggers Ca^{2+} mediated lysosomal exocytosis (see also Suppl. Fig. 3)

A-C) Incoming adenovirus induces Ca^{2+}-dependent lysosomal exocytosis. The activity of the lysosomal enzymes β-hexosaminidase or ASMase in the supernatant of cells under indicated conditions was determined at 37°C 45 min pi (A), or in cold-synchronized infections as indicated (B, C). SLO is a well established inducer of lysosomal exocytosis (Tam et al., 2010), and is used as positive control, while triton-x (T-X) is used to solubilize membranes and measure the total activity of lysosomal enzymes.

D) Lysosomal exocytosis accelerated endosomal escape. Cells were pre-treated with nocodazole and exposed to bSMase during 20 min of infection. Cytosolic HAdV-C2-Alexa488 was stained by immunofluorescence labeling in SLO-treated cells. Control

staining of surface bound viruses in absence of SLO is shown in Supplemental Fig. 3G.

Fig. 6: Protein-VI of incoming adenovirus permeabilizes the plasma membrane and triggers cytosolic Ca^{2+} influx (see also Suppl. Fig. 4)

A-C) Incoming adenovirus permeabilizes the PM. Cytosolic Ca^{2+} transients and propidium iodide influx were analyzed in cells expressing GCamP during the first minutes of infection, either by confocal microscopy or flow cytometry.

D) Endocytosis is not required for plasma membrane permeabilization by incoming HAdV. HeLa cells expressing Dyn2K44A-GFP, a dominant negative dynamin-2 mutant incapable of vesicle scission (Altschuler et al., 1998), were imaged by time-lapse confocal microscopy in presence of propidium iodide (PI). The expression of Dyn2K44A-GFP blocks HAdV endocytosis (Gastaldelli et al., 2008; Meier et al., 2002; Nakano et al., 2000). Influx of PI occurred in presence of DynK44A showing that endocytosis is not required for plasma membrane permeabilization.

E-G) Protein-VI permeabilizes the plasma membrane. In presence of propidium iodide, cells were exposed to HAdV-C5 or mutant VI-L40Q or to heat-uncoated HAdV-C2 pre-incubated with indicated antibodies.

Fig. 7: Schematic summary of lipid signaling enhanced virus penetration of endosomal membranes

1) Limited HAdV uncoating leads to exposure of the membrane-lytic protein-VI and influx of Ca^{2+} through small lesions of the plasma membrane. 2) Ca^{2+} influx triggers lysosomal exocytosis and delivery of ASMase to the outer surface of the plasma membrane. 3) ASMase converts sphingomyelin (SM) to ceramide (Cer). 4) Cer increase accelerates virus endocytosis. 5) Cer increasingly recruits protein-VI and this enhances the destabilization of the endosomal membrane until enough protein-VI has been released. 6) Endosomal membrane breaks and virus is released to the cytosol.

F1

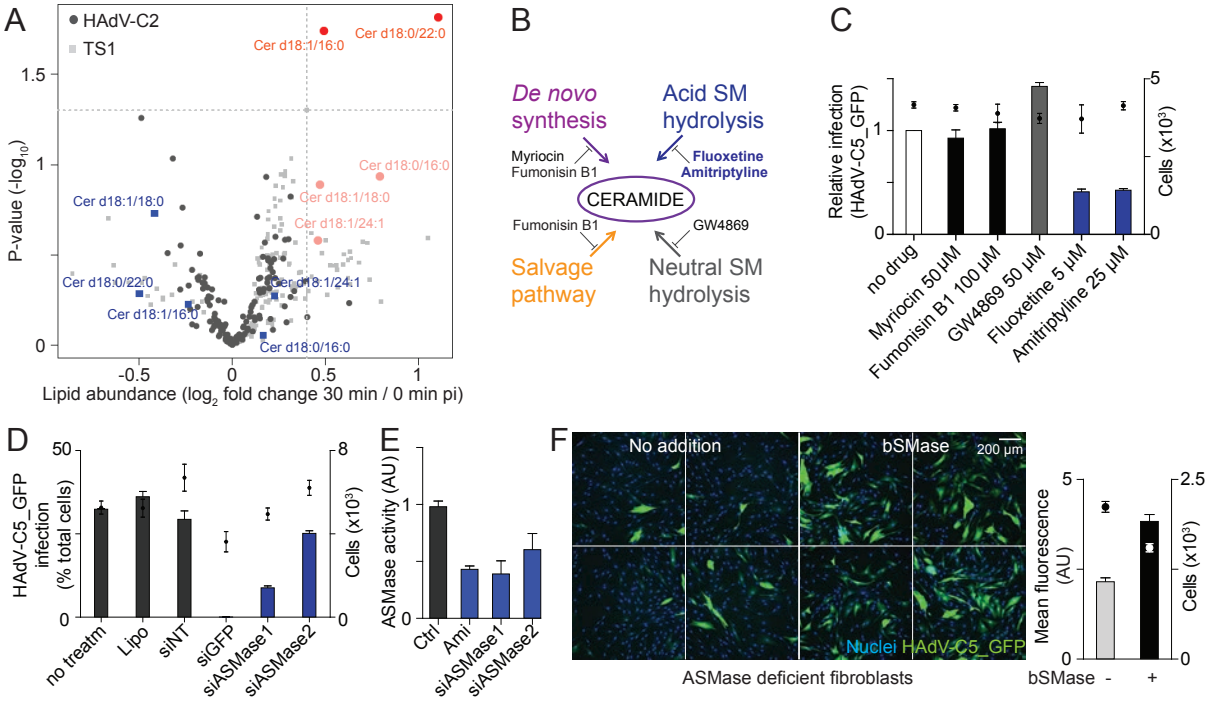
A
HAdV-C2
TS1
Cer d18:0/22:0
Cer d18:1/16:0
Cer d18:0/16:0
Cer d18:1/18:0
Cer d18:1/24:1
Cer d18:0/22:0
Cer d18:1/24:1
Cer d18:1/16:0
Cer d18:0/16:0
P-value (-log10)
Lipid abundance (log2 fold change 30 min / 0 min pi)
B
De novo synthesis
Acid SM hydrolysis
Myriocin
Fumonisin B1
Fluoxetine
Amitriptyline
CERAMIDE
Fumonisin B1
GW4869
Salvage pathway
Neutral SM hydrolysis
C
Relative infection (HAdV-C5_GFP)
Cells (x10³)
no drug
Myriocin 50 µM
Fumonisin B1 100 µM
GW4869 50 µM
Fluoxetine 5 µM
Amitriptyline 25 µM
D
HAdV-C5_GFP infection (% total cells)
Cells (x10³)
no treatm
Lipo
siNT
siGFP
siASMase1
siASMase2
E
ASMase activity (AU)
Ctrl
Ami
siASMase1
siASMase2
F
No addition
bSMase
200 µm
Nuclei HAdV-C5_GFP
ASMase deficient fibroblasts
Mean fluorescence (AU)
Cells (x10³)
bSMase - +

F2

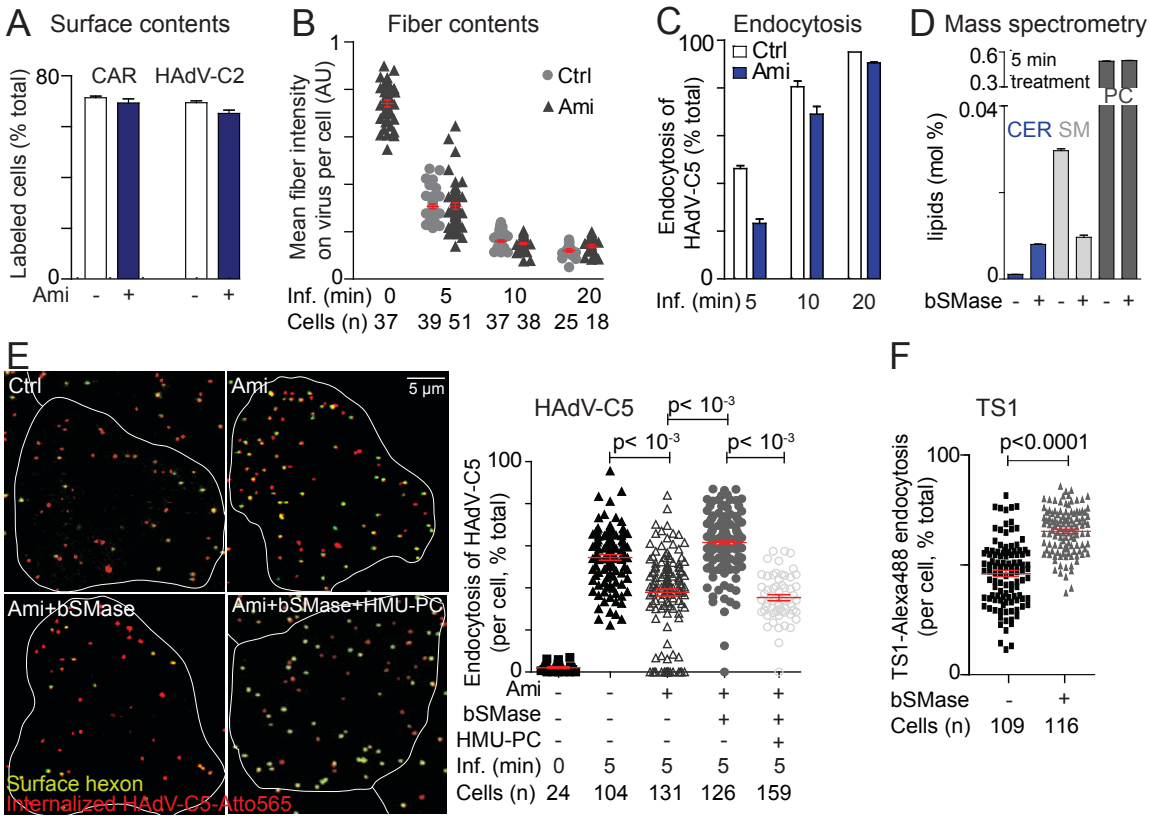
A Surface contents
Labeled cells (% total)
80
0
CAR HAdV-C2
Ami - + - +
B Fiber contents
Mean fiber intensity on virus per cell (AU)
1
0
Ctrl
Ami
Inf. (min) 0 5 10 20
Cells (n) 37 39 51 37 38 25 18
C Endocytosis
100
0
Ctrl
Ami
Endocytosis of HAdV-C5 (% total)
Inf. (min) 5 10 20
D Mass spectrometry
0.6
0.3
0.04
0
5 min treatment
PC
CER SM
lipids (mol %)
bSMase - + - + - +
E
Ctrl
Ami
5 µm
Ami+bSMase
Ami+bSMase+HMU-PC
Surface hexon
Internalized HAdV-C5-Atto565
HAdV-C5
p< 10-3
p< 10-3
p< 10-3
100
0
Endocytosis of HAdV-C5 (per cell, % total)
Ami - - + + +
bSMase - - - + +
HMU-PC - - - - +
Inf. (min) 0 5 5 5 5
Cells (n) 24 104 131 126 159
F
TS1
p<0.0001
100
0
TS1-Alexa488 endocytosis (per cell, % total)
bSMase - +
Cells (n) 109 116

F3

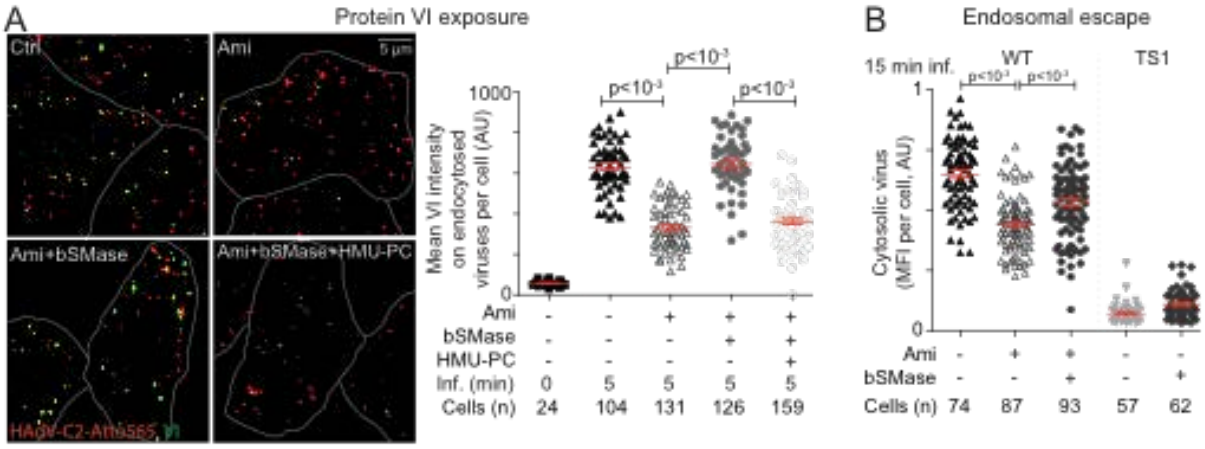
A
Protein VI exposure
Ctrl
Ami
5 µm
Ami+bSMase
Ami+bSMase+HMU-PC
HAdV-C2-Atto565, VI
Mean VI intensity on endocytosed viruses per cell (AU)
1000
0
p<10-3
p<10-3
p<10-3
Ami - - + + +
bSMase - - - + +
HMU-PC - - - - +
Inf. (min) 0 5 5 5 5
Cells (n) 24 104 131 126 159
B
Endosomal escape
15 min inf.
WT
TS1
p<10-3
p<10-3
Cytosolic virus (MFI per cell, AU)
1
0
Ami - + + - -
bSMase - - + - +
Cells (n) 74 87 93 57 62

F4

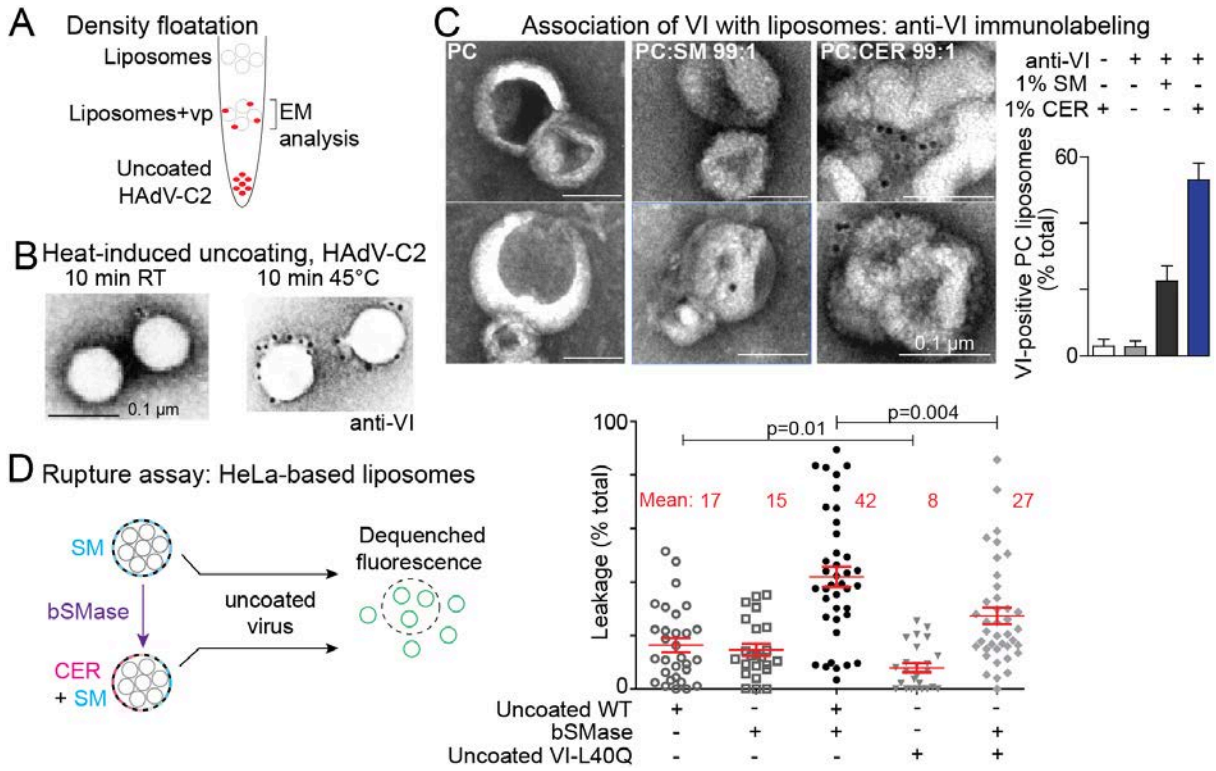
A
Density floatation
Liposomes
Liposomes+vp
EM analysis
Uncoated HAdV-C2
B Heat-induced uncoating, HAdV-C2
10 min RT
10 min 45°C
0.1 µm
anti-VI
C
Association of VI with liposomes: anti-VI immunolabeling
PC
PC:SM 99:1
PC:CER 99:1
0.1 µm
anti-VI - + + +
1% SM - - + -
1% CER + - - +
VI-positive PC liposomes (% total)
60
0
D Rupture assay: HeLa-based liposomes
SM
bSMase
CER + SM
uncoated virus
Dequenched fluorescence
Leakage (% total)
100
0
p=0.01
p=0.004
Mean: 17
15
42
8
27
Uncoated WT + - + - -
bSMase - + + - +
Uncoated VI-L40Q - - - + +

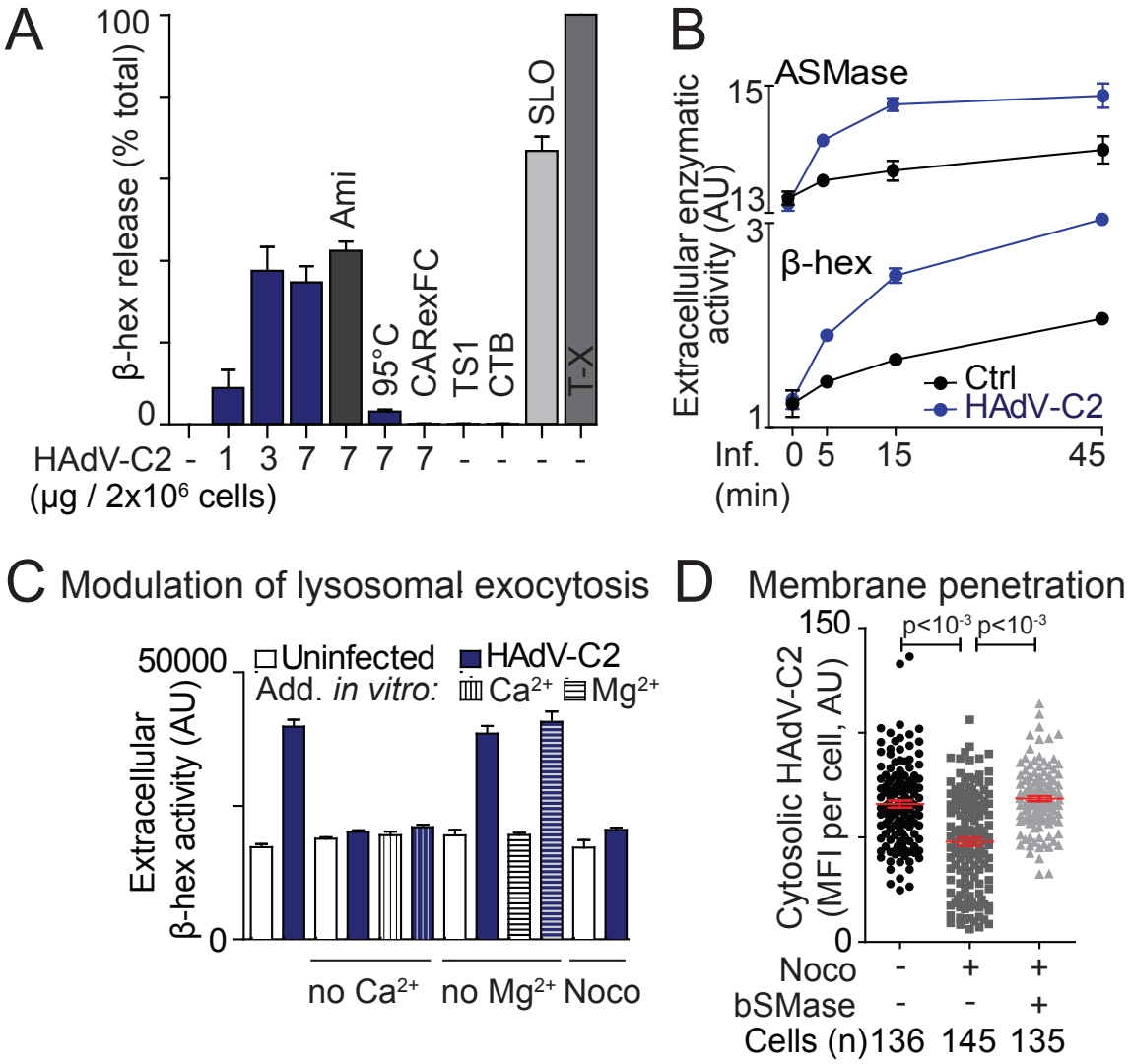
A
β-hex release (% total)
100
0
Ami
95°C
CARexFC
TS1
CTB
SLO
T-X
HAdV-C2 - 1 3 7 7 7 7 - - - -
(μg / 2x10⁶ cells)
B
ASMase
β-hex
Extracellular enzymatic activity (AU)
15
13
3
1
Ctrl
HAdV-C2
Inf. 0 5 15 45
(min)
C Modulation of lysosomal exocytosis
50000
0
Extracellular β-hex activity (AU)
Uninfected
HAdV-C2
Add. in vitro: Ca2+ Mg2+
no Ca2+
no Mg2+
Noco
D Membrane penetration
p<10-3 p<10-3
150
0
Cytosolic HAdV-C2 (MFI per cell, AU)
Noco - + +
bSMase - - +
Cells (n) 136 145 135

F6

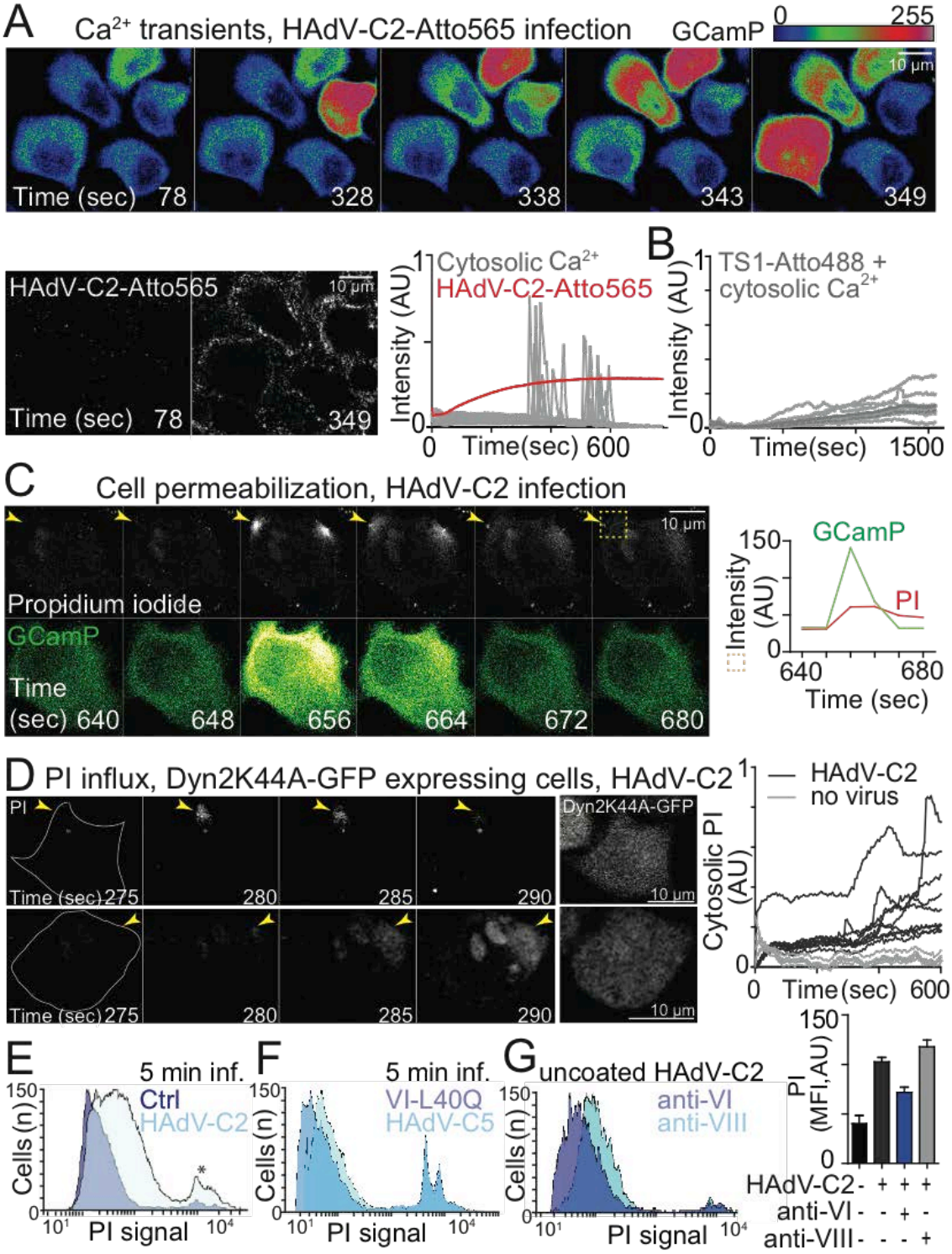
A
Ca2+ transients, HAdV-C2-Atto565 infection
GCamP
0
255
10 µm
Time (sec) 78
328
338
343
349
HAdV-C2-Atto565
10 µm
Time (sec) 78
349
Cytosolic Ca2+
HAdV-C2-Atto565
Intensity (AU)
1
0
0
Time(sec) 600
B
TS1-Atto488 +
cytosolic Ca2+
Intensity (AU)
1
0
0
Time(sec) 1500
C
Cell permeabilization, HAdV-C2 infection
10 µm
Propidium iodide
GCamP
Time
(sec) 640
648
656
664
672
680
GCamP
PI
150
Intensity (AU)
0
640
680
Time (sec)
D
PI influx, Dyn2K44A-GFP expressing cells, HAdV-C2
PI
Time (sec) 275
280
285
290
Dyn2K44A-GFP
10 µm
HAdV-C2
no virus
Cytosolic PI (AU)
1
0
0
Time(sec) 600
E
5 min inf.
Ctrl
HAdV-C2
Cells (n)
150
0
10¹
PI signal
10⁴
F
5 min inf.
VI-L40Q
HAdV-C5
Cells (n)
150
0
10¹
PI signal
10⁴
G
uncoated HAdV-C2
anti-VI
anti-VIII
Cells (n)
150
0
10¹
PI signal
10⁴
PI (MFI,AU)
150
0
HAdV-C2 - + + +
anti-VI - - + -
anti-VIII - - - +

F7

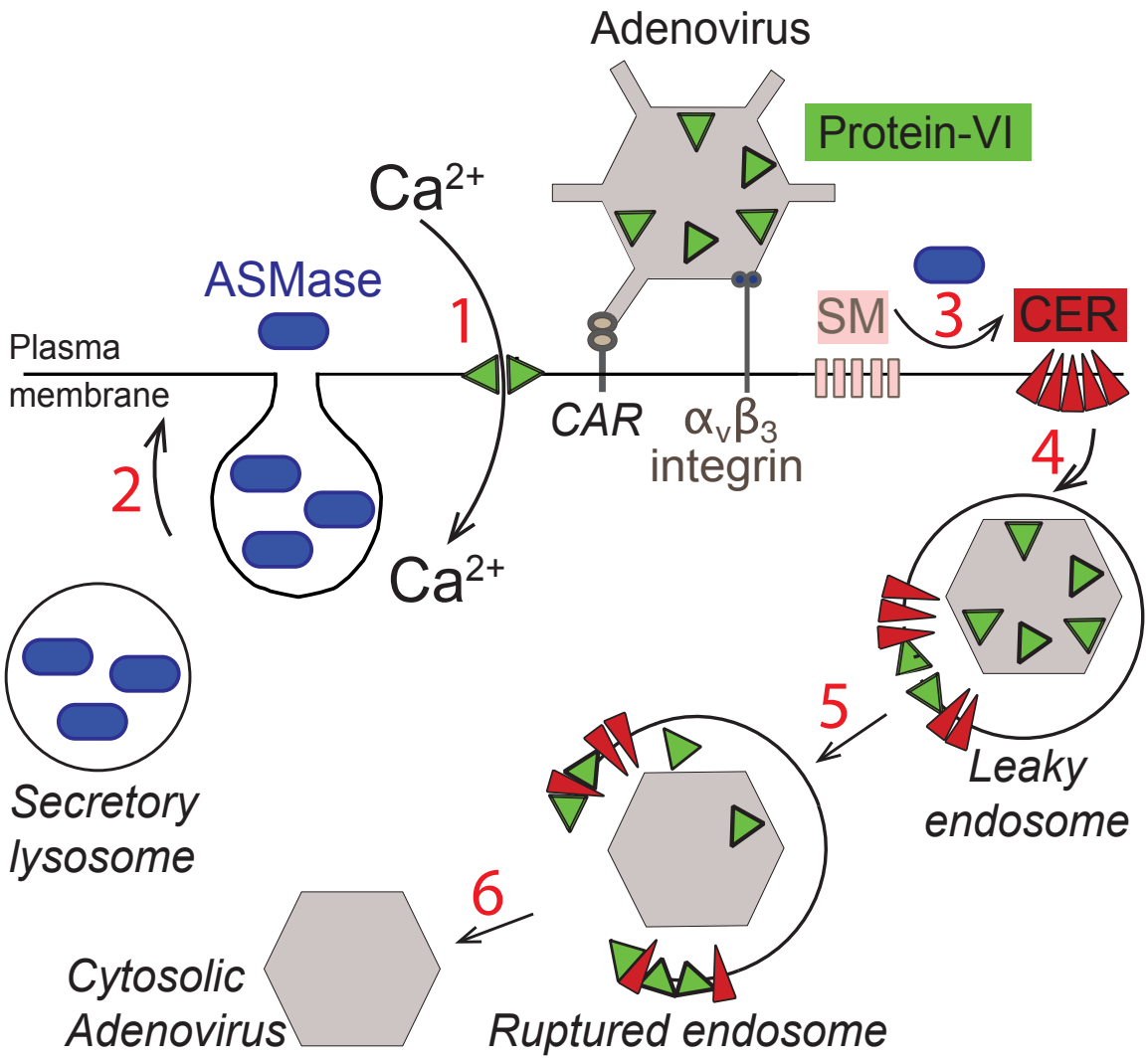
Adenovirus
Protein-VI
Ca2+
ASMase
1
Plasma
membrane
SM
3
CER
CAR
αvβ3
integrin
2
4
Ca2+
Secretory
lysosome
5
Leaky
endosome
6
Cytosolic
Adenovirus
Ruptured endosome

Supplemental Data

Supplemental Procedures

Cells and viruses

HeLa cervical carcinoma cells, subline Ohio (from L. Kaiser, University Hospital, Geneva, Switzerland), human bronchial epithelial A549 cells, and primary human embryonic lung Wi-38 cells (both American Type Culture Collection) were grown at 37°C under 5% CO_2 in Dulbecco's modified Eagle's medium (DMEM; Sigma) supplemented with 7.5% fetal calf serum (FCS; Life Technologies) and 1% nonessential amino acids (Sigma). Human Niemann-Pick disease A fibroblasts GM00112 (Coriell Institute for Medical Research, Camden, NJ) were cultured in Eagle's Minimum Essential Medium with Earle's salts, 1% non-essential amino acids and 10% fetal calf serum and human airway epithelial cells from nasal biopsies (hAECN) in hAEC medium (Epithelix, Geneva, Switzerland). HAdV-C2, the penetration-deficient mutant TS1, and HAdV-C5 were grown in A549 cells, isolated, and labeled with Alexa Fluor 488 (Alexa488; Life Technologies) or Atto-565 (Atto-Tec, Germany) as previously described (Burckhardt et al., 2011; Greber et al., 1996; Greber et al., 1993). HAdV-C5_GFP, an E1/E3 deletion mutant virus containing the enhanced green fluorescent protein (GFP) gene in the E1 region under the control of cytomegalovirus major immediate early promoter (Fleischli et al., 2007; Nagel et al., 2003), and the HAdV5-C5_GFP-VI_L40Q (VI-L40Q) (Moyer et al., 2011) were grown in adenovirus early region 1-transfected human embryonic retinoblast 911 cells (Yakimovich et al., 2012).

Fiber shedding, endocytosis and VI exposure

Fluorescently labeled HAdVs were exposed at 4°C for 1 h to cells pre-treated with amitriptyline (25 μM for 4 h), to yield 50-200 viruses per cell. Bound viruses were internalized at 37°C for indicated times. For the endocytosis assay, surface viruses were stained with 9C12 anti-hexon antibody (Varghese et al., 2004) at 4°C in intact cells. For fiber loss and protein-VI exposure, fixed and permeabilized samples were stained with R72 anti-fiber antibody (Baum et al., 1972) and affinity purified anti-protein-VI antibody (Burckhardt et al., 2011). Samples were processed for

fluorescence microscopy and images acquired with Leica SP5 equipped with 63× objective (oil immersion, numerical aperture 1.4). Maximum projection images of Z-stacks (11 x 0.5 µm steps, 16x frame averaging) were analyzed using a customized Matlab routine (available upon request). Fluorescence intensity of the antibody staining on the position of each virus was determined and mean values per cell are shown. Endocytosed viruses were identified as positive for the fluorescent tag but negative for surface staining with 9C12. Intensity of protein-VI staining was evaluated on endocytosed viruses only, to exclude effects due to internalization delay (Burckhardt et al., 2011; Suomalainen et al., 2013).

ASMase, β-hexosaminidase and lactate dehydrogenase activity measurements

Activity of ASMase was determined as previously described (van Diggelen et al., 2005). Briefly, for extracellular ASMase activity, cells were exposed to cold binding with the indicated ligands in RPMI-0.2% FAF-BSA (cholera toxin subunit B; CTB; Crucell; 1 mg/ml CARex-FC kindly provided by S. Hemmi (University of Zürich) (Ebbinghaus et al., 2001). Unbound ligands were removed and cells placed at 37°C in exocytosis buffer (25 mM HEPES, 125 mM NaCl, 5 mM KCl, 1.2 mM $MgSO_4$, 1 mM $CaCl_2$, 1.2 mM KH_2PO_4, 6 mM D-glucose) for 5, 15 or 45 min. For Ca^{2+}- and Mg^{2+}-free media, exocytosis buffer devoid of $CaCl_2$ and $MgSO_4$ were used. Supernatants were collected and cleared by centrifugation at 11'000 x *g* for 5 min. For total ASMase activity, lysates of cells treated with drugs and siRNA were resuspended in ultra pure H_2O containing 1 mM PMSF (Sigma), and protein concentration was determined using the Micro BCA kit (Thermo Scientifics). Equal protein amounts or volumes of supernatants were incubated with 0.4 mg/ml 6-hexadecanoylamino-4-methylumbelliferylphosphorylcholine (HMU-PC; Moscerdam Substrates) in substrate buffer (0.1 M sodium acetate buffer, 0.2% w/v), synthetic sodium taurocholate (Sigma), pH 5.2 at 37°C for 3 h. The reaction was stopped by adding 0.5 M sodium carbonate, 0.25% Triton X-100, pH 10.7 at RT in the dark for 15 min. Fluorescence was recorded with M200 Infinite Plate Reader (Tecan) at 404 nm excitation and 460 nm emission. For β-hexosaminidase and lactate dehydrogenase activity, supernatants were processed as described (Evans et al., 1985; Rodríguez et al., 1997).

Resazurin assay

Cell toxicity was evaluated using the resazurin fluorometric assay (Czekanska, 2011). Briefly, cells were placed into sterile filtered 0.002% resazurin (Sigma) in PBS at 37°C, for 90 min in a 5% CO_2 incubator. The reduction of resazurin to the fluorescent resorufin by mitochondrial enzymes was measured using M200 Infinite Plate Reader (Tecan) at excitation 550/9 nm and emission 590/20 nm.

Flow cytometry

Cells were harvested in PBS-20 mM EDTA, incubated with HAdV-C2/5, VI-L40Q, heat-treated HAdV-C2/5, HAdV-C5-Atto488 or anti-CAR antibody E1-1 (kindly provided by S. Hemmi, University of Zürich) at 4°C for 1 h. For PI accessibility, cells were placed in RPMI-0.2% FAF-BSA containing 0.2 mg/ml PI at 37°C for 5 min. For surface profiling, unbound antibodies or viruses were washed away, and cells fixed and stained with anti-CAR antibody. For protein-VI immuno-depletion, 1 μg heat treated virus were incubated with 12 μg of either anti-VI IgG or an anti-VIII IgG for 1 h (Burckhardt et al., 2011) and cells were incubated with PI at 37°C for 20 min. More than 5000 cells per samples were analyzed with FACSCanto II (BD Biosciences).

Lysotracker quantification

HeLa cells were loaded with LysoTracker Red DND99 as indicated by the manufacturer (Invitrogen). Time-lapse imaging of infection was performed as described above, except that Z-stacks were composed of 11 x 0.5 μm steps and were acquired at 0 min and 20 min pi. The total lysotracker signal on maximal projections was quantified using MacBiophotonics ImageJ.

Supplemental Figures

Supplemental Fig. 1: The ASMase inhibitor amitriptyline reduces infection (related to Fig. 1)

A) HeLa cells were pre-treated with amitriptyline (Ami, 25 µM) in DMEM-0.2% fatty-acid-free (FAF)-BSA and infected with HAdV-C2 for 18 h in presence or absence of the drug. Newly synthesized hexon was stained in fixed cells, and the percent infected cells plotted.

B) HeLa cells were incubated with amitriptyline in DMEM-0.2% FAF-BSA for 24 h and metabolic activity was assessed by resazurin assay.

C) Late addition of amitriptyline does not reduce HAdV-C5_GFP infection of HeLa cells.

D) Amitriptyline inhibits infection of HeLa cells with a B-species adenovirus. HeLa cells were pre-treated with amitriptyline (25 µM) in DMEM-0.2% FAF-BSA and infected with HAdV-B3_GFP for 22 h in presence of the drug, as described earlier (Sirena et al., 2005).

E, F) Inhibition of infection in primary nasal and A549 cells with HAdV-C5_GFP by amitriptyline. Cells were treated with the indicated drugs for 4 h before and 16 h during infection.

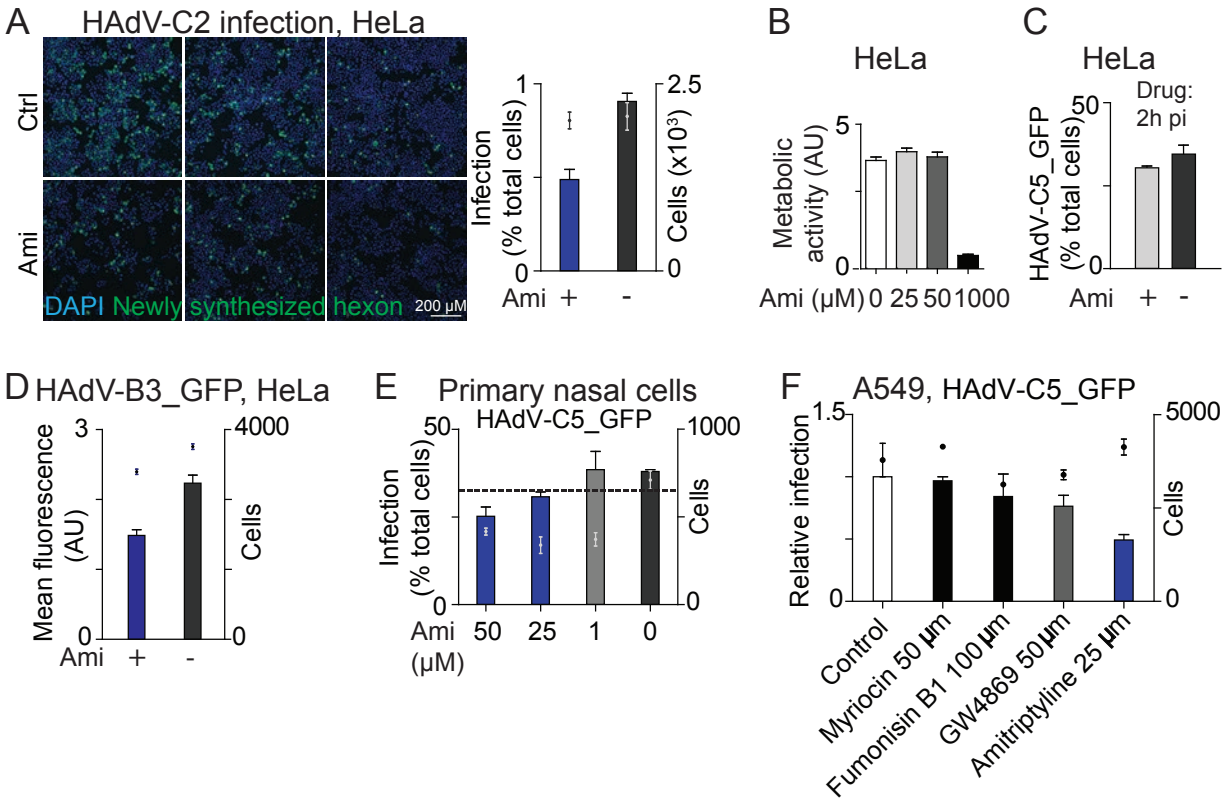

Supplemental Fig. 2: Amitriptyline reduces endosomal escape of HAdV (related to Fig. 2)

A) Control immune-fluorescence staining of surface-bound HAdV-C5-Atto565 viruses with anti-hexon antibody 9C12 in absence of permeabilization, parallel to the sample shown in Fig. 3 b. Per cell results show that most viruses were internalized at the time of SLO treatment.

B) HeLa cells were pretreated or not with amitriptyline (Ami), infected with HAdV-C2 at 37°C for 20 min upon cold-synchronized binding, and analyzed by thin section EM as described before (Suomalainen et al., 2013). The number of viruses at the plasma membrane, in endosomes and the cytosol were quantitated on a per cell basis.

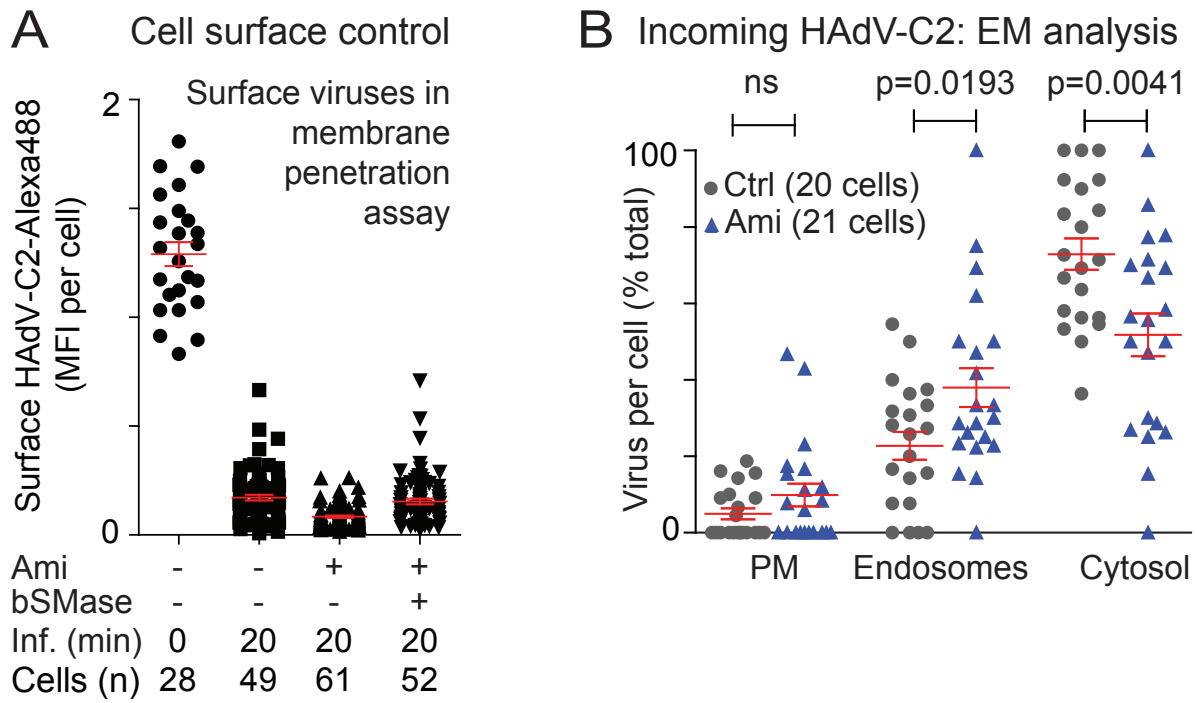

Supplemental Fig. 3: HAdV-C2/5 but not TS1 induces lysosomal exocytosis depending on extracellular Ca^{2+} (related to Fig. 5)

A, B) The supernatants of HeLa and Wi38 cells exposed to synchronized internalization of HAdV-C2 or cholera toxin B subunit (CTB) were collected 15 and 45 min post warming, respectively. Note that the kinetics of HAdV-C2 endocytosis in Wi38 cells is slightly slower compared to HeLa (data not shown). Enzymatic activities of cell-free lysosomal ASMase and cytosolic lactate dehydrogenase (LDH) were measured, and compared to the total activities in Triton-X100 (Tx) extracted cells.

C) Lysotracker-labeled cells were infected and subjected to live imaging. The intensity of the lysotracker signal per cell was determined at 0 and 20 min pi. The ratio of the signals at 20 min over 0 min are shown for individual cells (n). Note the significant reduction of the lysotracker signal in HAdV-C2 inoculated cells.

D) Reduced infection of HeLa cells with HAdV-C5_GFP in medium devoid of extracellular Ca^{2+} compared to normal medium for 2 h, followed by incubation in normal medium for 14 h. Virus binding in presence or absence of Ca^{2+} was equally efficient (data not shown, and Greber et al., 1997).

E, F) Endocytosis of HAdV-C5-Atto565 but not that of TS1-Alexa488 is delayed in absence of extracellular Ca^{2+}. Viruses were cold-bound to cells in full media. Unbound viruses were washed away in media with or without Ca^{2+} and internalized in corresponding warm medium as indicated.

G) Control staining of surface HAdV-C2-Alexa488 with anti-Alexa488 in the absence of SLO permeabilization, parallel to SLO-permeabilized samples in Fig. 5d. Note that neither nocodazole (noco) nor bSMase treatment significantly enlarged the cell surface contents of HAdV-C2-Alexa488 20 min pi.

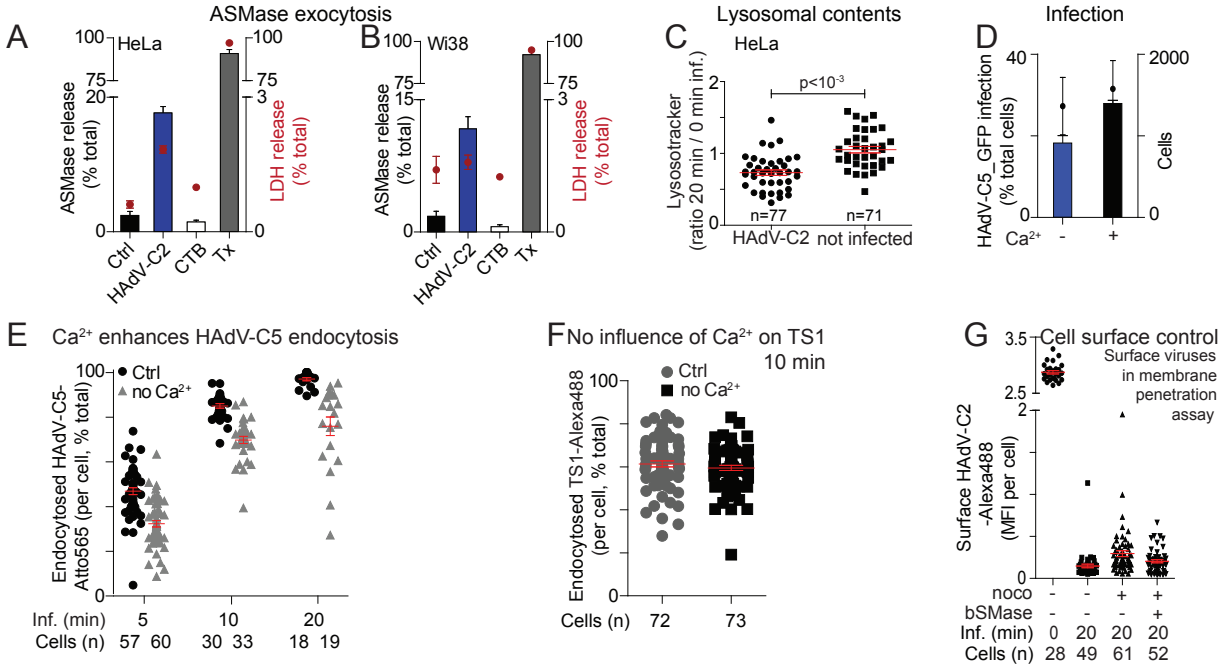
A
ASMase exocytosis
HeLa
ASMase release (% total)
LDH release (% total)
Ctrl
HAdV-C2
CTB
Tx
B
Wi38
C
Lysosomal contents
HeLa
Lysotracker (ratio 20 min / 0 min inf.)
p<10-3
n=77
n=71
HAdV-C2
not infected
D
Infection
HAdV-C5_GFP infection (% total cells)
Cells
Ca2+
E
Ca2+ enhances HAdV-C5 endocytosis
Endocytosed HAdV-C5-Atto565 (per cell, % total)
Ctrl
no Ca2+
Inf. (min)
Cells (n)
F
No influence of Ca2+ on TS1
10 min
Endocytosed TS1-Alexa488 (per cell, % total)
G
Cell surface control
Surface viruses in membrane penetration assay
Surface HAdV-C2 -Alexa488 (MFI per cell)
noco
bSMase

Supplemental Fig. 4: HAdV-C2/5 induces protein-VI dependent influx of extracellular Ca^{2+} (related to Fig. 6)

A) Determination of the fraction of broken particles in HAdV-C2/5 inocula. Viruses were cold bound to cells and internalized at 37°C for 15 min. Samples were fixed, stained for protein-VI and analyzed by confocal microscopy. To estimate background values of the protein-VI staining, uninfected cells were recorded under the same conditions as infected cells, and Atto565 images superimposed onto protein-VI images. The intensity of protein-VI staining (raw values) associated to single viruses was quantified using Matlab. The second highest value of signal intensity associated to a virus mask projected onto the images of uninfected cells was used as threshold to estimate the % of broken particles (thresholded values). Protein-VI signals on viruses bound to cells at 4°C represent broken particles in the inoculum. Note that the level of protein-VI positive particles is greatly enhanced by temperature shift to 37°C indicative of virus uncoating (Burckhardt et al., 2011). We estimate that approximately three out of 1000 viruses in the inoculum are broken. The plot shows a representative population of 323 viruses.

B-E) HeLa cells expressing the cytosolic Ca^{2+} sensor GCamP (Akerboom et al., 2012) were infected with HAdV in medium with or without extracellular Ca^{2+} or propidium iodide (PI). Confocal time-lapse imaging was performed and the cytosolic signal intensity profile quantified.

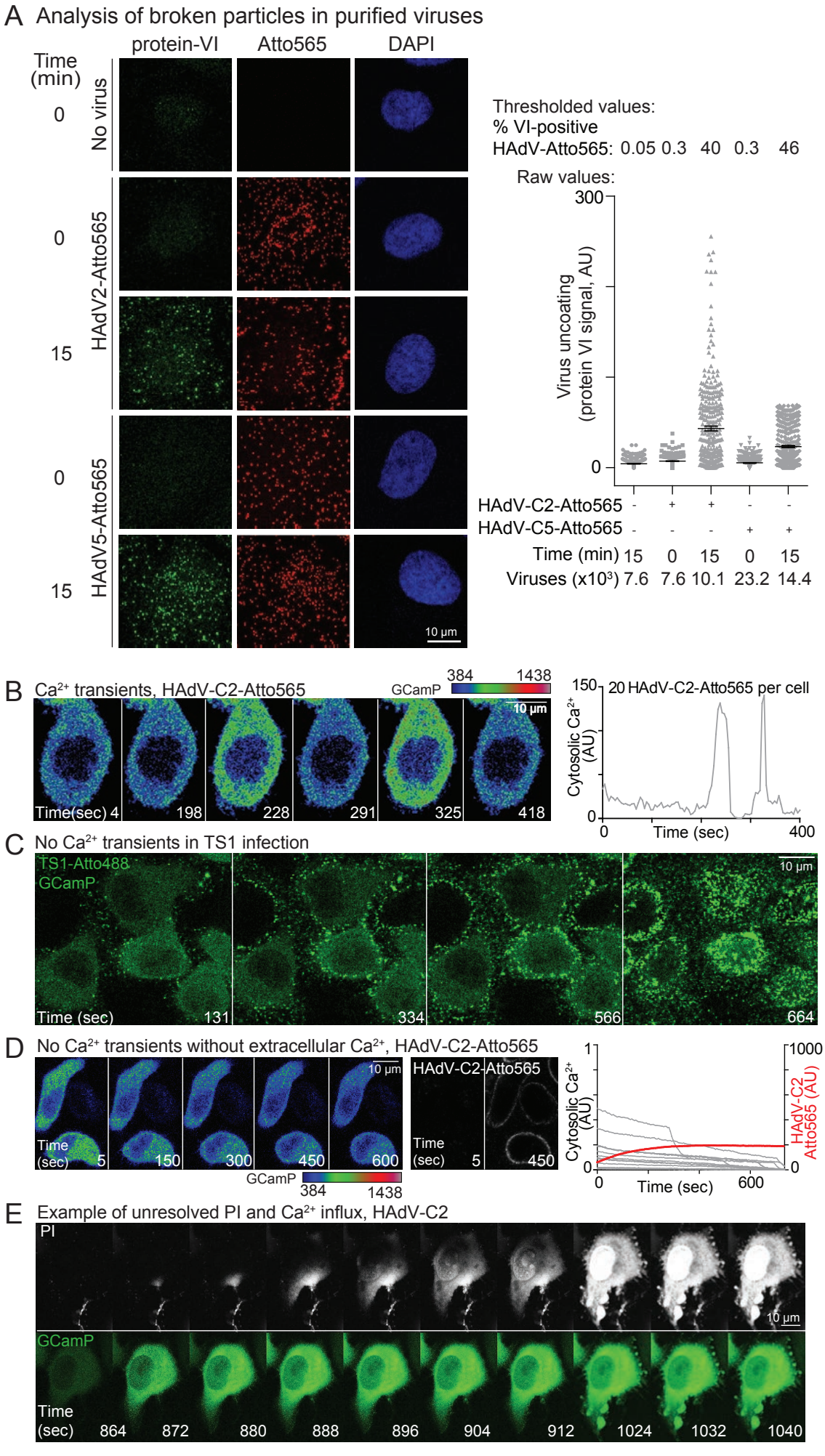
A Analysis of broken particles in purified viruses
protein-VI
Atto565
DAPI
Time (min)
No virus
HAdV2-Atto565
HAdV5-Atto565
0
0
15
0
15
10 µm
Thresholded values:
% VI-positive
HAdV-Atto565: 0.05 0.3 40 0.3 46
Raw values:
Virus uncoating (protein VI signal, AU)
300
0
HAdV-C2-Atto565 - + + - -
HAdV-C5-Atto565 - - - + +
Time (min) 15 0 15 0 15
Viruses (x10³) 7.6 7.6 10.1 23.2 14.4
B Ca²⁺ transients, HAdV-C2-Atto565
GCamP 384 1438
10 µm
Time(sec) 4 198 228 291 325 418
150
20 HAdV-C2-Atto565 per cell
Cytosolic Ca²⁺ (AU)
0
Time (sec)
400
C No Ca²⁺ transients in TS1 infection
TS1-Atto488
GCamP
10 µm
Time (sec) 131 334 566 664
D No Ca²⁺ transients without extracellular Ca²⁺, HAdV-C2-Atto565
10 µm
Time (sec) 5 150 300 450 600
GCamP 384 1438
HAdV-C2-Atto565
Time (sec) 5 450
1
1000
Cytosolic Ca²⁺ (AU)
HAdV-C2 Atto565 (AU)
0
0
Time (sec)
600
E Example of unresolved PI and Ca²⁺ influx, HAdV-C2
PI
10 µm
GCamP
Time (sec) 864 872 880 888 896 904 912 1024 1032 1040

Supplemental Table 1 (related to Fig. 1)

Lipid species were identified, analyzed and quantified as previously described (Tanner et al., 2014). The listed values represent the molar fraction of each lipid species normalized to the total amount of measured phospholipids.

		TS1						HAdV-C2					
		not infected			infected			not infected			Infected		
Lipid species	m/z	TS1_K_1	TS1_K_2	TS1_K_3	TS1_30min_1	TS1_30min_2	TS1_30min_3	HAdV-C2_K_1	HAdV-C2_K_2	HAdV-C2_K_3	HAdV-C2_30min_1	HAdV-C2_30min_2	HAdV-C2_30min_3
PC 32:0a	734.6/184.1	0.01479049	0.01842064	0.01402803	0.01919385	0.01721029	0.01699880	0.01631976	0.01630837	0.01213584	0.01750453	0.01898288	0.01312402
PC 34:0a	762.6/184.1	0.00477552	0.00556840	0.00421316	0.00554755	0.00511099	0.00558282	0.00472436	0.00457394	0.00356317	0.00527282	0.00561252	0.00421904
PC 36:0a	790.6/184.1	0.00123665	0.00155067	0.00123109	0.00165862	0.00141548	0.00139736	0.00140435	0.00137607	0.00105365	0.00144028	0.00163773	0.00116025
PC 38:0a	818.7/184.1	0.00276343	0.00399867	0.00311578	0.00493053	0.00379396	0.00258330	0.00399358	0.00361983	0.00260140	0.00366680	0.00411747	0.00271145
PC 40:0a	846.7/184.1	0.00039017	0.00056894	0.00040827	0.00078548	0.00059069	0.00033207	0.00070447	0.00061780	0.00037201	0.00054774	0.00059210	0.00035002
PC 32:1a	732.6/184.1	0.02576230	0.03087279	0.02378852	0.03351810	0.03063577	0.03225912	0.02887578	0.02817850	0.02228665	0.02738279	0.03035190	0.02150358
PC 34:1a	760.6/184.1	0.03136492	0.03652948	0.02797692	0.03648429	0.03453477	0.03849764	0.03184854	0.03113447	0.02392987	0.03454905	0.03722688	0.02759191
PC 36:1a	788.6/184.1	0.00721692	0.00801140	0.00613092	0.00832303	0.00741357	0.00774085	0.00691410	0.00666031	0.00500591	0.00764123	0.00825936	0.00581481
PC 38:1a	816.6/184.1	0.00097696	0.00123183	0.00096751	0.00141789	0.00120646	0.00099652	0.00120023	0.00116594	0.00086306	0.00116157	0.00133682	0.00090567
PC 40:1a	844.7/184.1	0.00017252	0.00023965	0.00017735	0.00029076	0.00023283	0.00019122	0.00024718	0.00023981	0.00017063	0.00020575	0.00024147	0.00017731
PC 32:2a	730.5/184.1	0.00249957	0.00259323	0.00193806	0.00299826	0.00276164	0.00299620	0.00309316	0.00290953	0.00226373	0.00264834	0.00284917	0.00207662
PC 34:2a	758.6/184.1	0.01441863	0.01697096	0.01263825	0.01757607	0.01637891	0.01773322	0.01684841	0.01581561	0.01263659	0.01584151	0.01757948	0.01262768
PC 36:2a	786.6/184.1	0.02869826	0.03238920	0.02511275	0.03529174	0.03085159	0.03254776	0.03018764	0.02940611	0.02266495	0.03095480	0.03346632	0.02389389
PC 38:2a	814.6/184.1	0.00299358	0.00379737	0.00281547	0.00433063	0.00362832	0.00319617	0.00344220	0.00333301	0.00250592	0.00320618	0.00365874	0.00245649
PC 40:2a	842.7/184.1	0.00034396	0.00046137	0.00038372	0.00057126	0.00048543	0.00042527	0.00050493	0.00046554	0.00034324	0.00044243	0.00049136	0.00034773
PC 34:3a	756.6/184.1	0.00145230	0.00171974	0.00126397	0.00180763	0.00159919	0.00164740	0.00173326	0.00162121	0.00123399	0.00176024	0.00191076	0.00140125
PC 36:3a	784.6/184.1	0.00610296	0.00742772	0.00584400	0.00788005	0.00692728	0.00657361	0.00744495	0.00694409	0.00526357	0.00810691	0.00848418	0.00606308
PC 38:3a	812.6/184.1	0.00202949	0.00253446	0.00204114	0.00281482	0.00238295	0.00201898	0.00247062	0.00237395	0.00169375	0.00263358	0.00285717	0.00195995
PC 40:3a	840.6/184.1	0.00031532	0.00043663	0.00032588	0.00052166	0.00037189	0.00033720	0.00043596	0.00041891	0.00029919	0.00037816	0.00045656	0.00030967
PC 36:4a	782.6/184.1	0.00338321	0.00435088	0.00359649	0.00468146	0.00410206	0.00377677	0.00463246	0.00447021	0.00330587	0.00493084	0.00545731	0.00394916
PC 38:4a	810.6/184.1	0.00310358	0.00405858	0.00324322	0.00452903	0.00353987	0.00321306	0.00413351	0.00393273	0.00278480	0.00466991	0.00497308	0.00356318
PC 40:4a	838.6/184.1	0.00054294	0.00074481	0.00057872	0.00085881	0.00067446	0.00055768	0.00072141	0.00069660	0.00050507	0.00072499	0.00085886	0.00057362
PC 38:5a	808.6/184.1	0.00427390	0.00566190	0.00456745	0.00639481	0.00508399	0.00443429	0.00620406	0.00597722	0.00437642	0.00655425	0.00728744	0.00504151
PC 40:5a	836.6/184.1	0.00130968	0.00177534	0.00137943	0.00200475	0.00159430	0.00135665	0.00174183	0.00173103	0.00125611	0.00184957	0.00214315	0.00143893
PC 38:6a	806.6/184.1	0.00249269	0.00326111	0.00270386	0.00379507	0.00307633	0.00257727	0.00366646	0.00358253	0.00258611	0.00382061	0.00431937	0.00292261
PC 40:6a	834.6/184.1	0.00209998	0.00279498	0.00228099	0.00313915	0.00258643	0.00211460	0.00288604	0.00291905	0.00203484	0.00313483	0.00357076	0.00241077
PC 32:0e	720.6/184.1	0.00816217	0.00988887	0.00738008	0.01014071	0.00926111	0.00962351	0.00821599	0.00788849	0.00596229	0.00826981	0.00916405	0.00654011
PC 34:0e	748.6/184.1	0.00404810	0.00470354	0.00357214	0.00508233	0.00466171	0.00467889	0.00413630	0.00407338	0.00308579	0.00423879	0.00461358	0.00331893
PC 36:0e	776.7/184.1	0.00074300	0.00096676	0.00080822	0.00117908	0.00096194	0.00086653	0.00104474	0.00096953	0.00077316	0.00084182	0.00096349	0.00071267
PC 38:0e	804.7/184.1	0.00051050	0.00070147	0.00056106	0.00082803	0.00067765	0.00058633	0.00084600	0.00079024	0.00060863	0.00076077	0.00083443	0.00057362
PC 32:1e	718.6/184.1	0.00713066	0.00853472	0.00652154	0.00918334	0.00880013	0.00904079	0.00765346	0.00725032	0.00558236	0.00699729	0.00755139	0.00522914
PC 34:1e	746.6/184.1	0.01666866	0.01986625	0.01560936	0.02117637	0.01994450	0.02014038	0.01818737	0.01749944	0.01309923	0.01726422	0.01874099	0.01356318
PC 36:1e	774.6/184.1	0.00508197	0.00628984	0.00489070	0.00732439	0.00641782	0.00603433	0.00581156	0.00556041	0.00415005	0.00515560	0.00573531	0.00406354
PC 38:1e	802.7/184.1	0.00077109	0.00095087	0.00076378	0.00112670	0.00095556	0.00089066	0.00098713	0.00090862	0.00070627	0.00089538	0.00098273	0.00067193
PC 34:2e	744.6/184.1	0.00637987	0.00805134	0.00611550	0.00899349	0.00821029	0.00760543	0.00750774	0.00710701	0.00531283	0.00617588	0.00714693	0.00486688
PC 36:2e	772.6/184.1	0.01239421	0.01551446	0.01215693	0.01921416	0.01647799	0.01457807	0.01478424	0.01414835	0.01060373	0.01189013	0.01354524	0.00933362
PC 38:2e	800.7/184.1	0.00173718	0.00226372	0.00177552	0.00251423	0.00212673	0.00194720	0.00201134	0.00197674	0.00146684	0.00185665	0.00205322	0.00142783
PC 34:3e	742.6/184.1	0.00095286	0.00121889	0.00090501	0.00132596	0.00115650	0.00111807	0.00111850	0.00107725	0.00079006	0.00102534	0.00113210	0.00077044
PC 38:3e	798.6/184.1	0.00151518	0.00197891	0.00155759	0.00227991	0.00182182	0.00153369	0.00179585	0.00171428	0.00125665	0.00175923	0.00197886	0.00134425
PC 40:4e	824.7/184.1	0.00056033	0.00082560	0.00063188	0.00097640	0.00075462	0.00055708	0.00080972	0.00077939	0.00056710	0.00076380	0.00086232	0.00058624
PC 40:5e	822.6/184.1	0.00152751	0.00217566	0.00171221	0.00282102	0.00204657	0.00151439	0.00222344	0.00211358	0.00149381	0.00195831	0.00228907	0.00146838
PC 40:6e	820.6/184.1	0.00277974	0.00397575	0.00321420	0.00494913	0.00385541	0.00276336	0.00375716	0.00370377	0.00274632	0.00358899	0.00421669	0.00284668
SM d18:0/16:0	705.6/184.1	0.00066432	0.00088759	0.00102106	0.00096949	0.00089044	0.00109515	0.00087254	0.00102026	0.00098945	0.00078282	0.00115719	0.00099004
SM d18:0/18:0	733.6/184.1	0.00022952	0.00042953	0.00047982	0.00040756	0.00044678	0.00042022	0.00038077	0.00056194	0.00053492	0.00030566	0.00061522	0.00052237
SM d18:0/20:0	761.7/184.1	0.00017268	0.00029140	0.00038991	0.00029552	0.00030016	0.00032432	0.00028836	0.00042684	0.00041765	0.00021893	0.00050797	0.00040678
SM d18:0/22:0	789.7/184.1	0.00046658	0.00055931	0.00077769	0.00078663	0.00056019	0.00069809	0.00064508	0.00077493	0.00085308	0.00051544	0.00090768	0.00081001
SM d18:0/24:0	817.7/184.1	0.00040290	0.00043915	0.00055277	0.00065311	0.00045026	0.00047592	0.00051819	0.00062662	0.00057957	0.00040589	0.00064812	0.00051751
SM d18:0/26:0	845.7/184.1	0.00002448	0.00003854	0.00004775	0.00005329	0.00004640	0.00003709	0.00004215	0.00006138	0.00005001	0.00003325	0.00005841	0.00003897
SM d18:0/26:1	843.7/184.1	0.00004854	0.00005800	0.00007184	0.00008091	0.00006232	0.00006386	0.00007322	0.00009253	0.00008931	0.00005611	0.00009092	0.00007275
SM d18:1/16:0	703.6/184.1	0.00501953	0.00737416	0.00850760	0.00797685	0.00757097	0.00943790	0.00755567	0.00884428	0.00884318	0.00661715	0.00941406	0.00840823
SM d18:1/17:0	717.6/184.1	0.00027690	0.00051435	0.00058237	0.00048064	0.00052507	0.00052993	0.00048015	0.00061270	0.00060263	0.00042640	0.00067685	0.00063830
SM d18:1/18:0	731.6/184.1	0.00134540	0.00339012	0.00353983	0.00245920	0.00337044	0.00305715	0.00242977	0.00414790	0.00383620	0.00208986	0.00443200	0.00367597
SM d18:1/19:0	745.6/184.1	0.00010912	0.00028211	0.00031322	0.00019313	0.00028375	0.00024798	0.00019271	0.00036809	0.00031328	0.00015875	0.00041627	0.00031070
SM d18:1/20:0	759.6/184.1	0.00068786	0.00149578	0.00208193	0.00120665	0.00152985	0.00174559	0.00107962	0.00236479	0.00210751	0.00085510	0.00250752	0.00192207
SM d18:1/21:0	773.7/184.1	0.00026989	0.00045248	0.00072194	0.00046417	0.00045746	0.00063796	0.00038185	0.00066999	0.00071889	0.00031766	0.00074257	0.00066862
SM d18:1/22:0	787.7/184.1	0.00242033	0.00303186	0.00446481	0.00356321	0.00310491	0.00473204	0.00300054	0.00419199	0.00460704	0.00255855	0.00461776	0.00453220
SM d18:1/23:0	801.7/184.1	0.00070030	0.00074255	0.00094708	0.00101508	0.00076378	0.00098364	0.00083622	0.00101505	0.00104754	0.00066514	0.00105497	0.00094695

SM d18:1/24:0	815.7/184.1	0.00197992	0.00209263	0.00254779	0.00280282	0.00220814	0.00290123	0.00230504	0.00283459	0.00272078	0.00198192	0.00298825	0.00262200
SM d18:1/16:1	701.6/184.1	0.00058160	0.00096484	0.00102245	0.00092722	0.00100156	0.00105134	0.00089772	0.00113095	0.00111821	0.00075926	0.00116331	0.00102802
SM d18:1/18:1	729.6/184.1	0.00036838	0.00104043	0.00115769	0.00071486	0.00109431	0.00094763	0.00069593	0.00143832	0.00122996	0.00054665	0.00145200	0.00112294
SM d18:1/20:1	757.6/184.1	0.00017852	0.00032624	0.00049025	0.00031807	0.00033058	0.00043763	0.00027690	0.00051673	0.00048459	0.00022016	0.00055908	0.00047780
SM d18:1/24:1	813.7/184.1	0.00551993	0.00558211	0.00682058	0.00745237	0.00591075	0.00820580	0.00625621	0.00775966	0.00728698	0.00554291	0.00836310	0.00725415
SM d18:1/18:2	727.6/184.1	0.00001233	0.00002969	0.00003857	0.00002618	0.00002993	0.00002965	0.00002362	0.00004396	0.00004248	0.00002018	0.00004711	0.00003774
GlcCer d18:0/16:0	702.6/266.4	0.00001439	0.00002955	0.00001781	0.00004828	0.00002184	0.00002318	0.00002883	0.00002404	0.00002296	0.00001940	0.00002268	0.00001876
GlcCer d18:0/18:0	730.6/266.4	0.00000221	0.00001182	0.00000623	0.00001380	0.00001001	0.00000773	0.00000887	0.00000620	0.00000933	0.00000522	0.00001040	0.00000903
GlcCer d18:0/20:0	758.7/264.4	0.00002602	0.00003152	0.00001603	0.00004445	0.00003639	0.00002318	0.00004361	0.00002559	0.00002655	0.00002238	0.00003591	0.00002988
GlcCer d18:0/22:0	786.7/266.4	0.00003876	0.00004630	0.00003383	0.00006744	0.00006642	0.00003201	0.00005766	0.00003723	0.00002726	0.00005297	0.00003308	0.00004099
GlcCer d18:0/24:0	814.7/266.4	0.00005149	0.00008668	0.00004096	0.00009657	0.00007460	0.00005409	0.00010275	0.00005739	0.00005739	0.00006715	0.00005387	0.00005836
GlcCer d18:1/16:0	700.6/264.4	0.00091241	0.00165779	0.00091617	0.00183477	0.00137927	0.00098906	0.00144593	0.00123938	0.00104028	0.00118028	0.00122296	0.00099705
GlcCer d18:1/18:0	728.6/264.4	0.00024416	0.00049152	0.00024218	0.00053265	0.00039486	0.00024837	0.00041397	0.00030558	0.00029630	0.00032006	0.00029487	0.00029529
GlcCer d18:1/20:0	756.6/264.4	0.00012346	0.00022951	0.00011575	0.00027131	0.00021835	0.00012142	0.00020181	0.00013728	0.00013847	0.00018652	0.00015122	0.00015981
GlcCer d18:1/22:0	784.7/264.4	0.00142232	0.00265561	0.00122780	0.00263950	0.00246195	0.00154761	0.00221251	0.00155193	0.00169746	0.00203677	0.00181270	0.00161959
GlcCer d18:1/24:0	812.7/264.4	0.00222677	0.00423952	0.00214308	0.00440606	0.00404866	0.00266031	0.00403988	0.00259897	0.00269828	0.00307530	0.00289483	0.00281674
GlcCer d18:1/26:0	840.7/264.4	0.00003931	0.00010737	0.00003205	0.00008584	0.00009917	0.00004967	0.00007171	0.00005429	0.00005955	0.00005819	0.00005576	0.00005072
GlcCer d18:1/24:1	810.7/264.4	0.00279371	0.00549640	0.00269866	0.00545986	0.00495211	0.00328068	0.00482642	0.00320857	0.00338559	0.00429140	0.00396563	0.00397151
Cer d18:0/16:0	540.5/266.4	0.00008378	0.00002627	0.00032430	0.00018177	0.00005182	0.00025350	0.00018160	0.00021684	0.00011741	0.00038942	0.00029000	0.00021358
Cer d18:0/18:0	568.6/266.4	0.00004189	0.00007880	0.00000000	0.00003635	0.00007773	0.00003621	0.00012107	0.00000000	0.00003914	0.00002596	0.00007909	0.00014238
Cer d18:0/20:0	596.6/266.4	0.00000000	0.00005253	0.00000000	0.00007271	0.00000000	0.00000000	0.00003027	0.00006505	0.00001957	0.00000000	0.00000000	0.00002373
Cer d18:0/22:0	624.6/266.4	0.00004189	0.00018387	0.00016215	0.00010906	0.00012955	0.00003621	0.00006053	0.00006505	0.00009784	0.00012981	0.00018455	0.00016611
Cer d18:0/24:0	652.7/266.4	0.00010473	0.00005253	0.00016215	0.00039990	0.00015546	0.00000000	0.00006053	0.00017347	0.00007827	0.00005192	0.00007909	0.00014238
Cer d18:0/26:0	680.7/266.4	0.00000000	0.00000000	0.00003243	0.00003635	0.00000000	0.00000000	0.00000000	0.00002168	0.00000000	0.00000000	0.00000000	0.00000000
Cer d18:0/24:1	650.6/266.4	0.00004189	0.00013134	0.00022701	0.00014542	0.00007773	0.00007243	0.00021187	0.00015179	0.00011741	0.00010385	0.00018455	0.00021358
Cer d18:0/26:1	678.7/266.4	0.00000000	0.00000000	0.00003243	0.00000000	0.00000000	0.00000000	0.00000000	0.00000000	0.00000000	0.00002596	0.00000000	0.00000000
Cer d18:1/16:0	538.5/264.4	0.00289053	0.00462302	0.00671295	0.00487154	0.00380879	0.00340412	0.00514539	0.00516077	0.00448117	0.00636052	0.00767195	0.00676323
Cer d18:1/18:0	566.6/264.4	0.00079594	0.00123456	0.00119990	0.00079980	0.00093276	0.00068807	0.00160415	0.00175640	0.00109583	0.00184325	0.00250459	0.00182726
Cer d18:1/20:0	594.6/264.4	0.00010473	0.00044654	0.00038916	0.00047261	0.00031092	0.00028971	0.00036320	0.00060715	0.00029353	0.00028557	0.00073819	0.00026104
Cer d18:1/22:0	622.6/264.4	0.00171756	0.00210137	0.00236737	0.00330828	0.00212463	0.00181070	0.00311750	0.00199492	0.00211339	0.00277786	0.00445553	0.00270529
Cer d18:1/24:0	650.6/264.4	0.00232499	0.00438662	0.00385914	0.00618031	0.00370514	0.00365762	0.00499405	0.00438015	0.00322879	0.00371247	0.00471917	0.00443763
Cer d18:1/26:0	678.7/264.4	0.00006284	0.00010507	0.00009729	0.00003635	0.00002591	0.00010864	0.00006053	0.00017347	0.00005871	0.00005192	0.00010546	0.00009492
Cer d18:1/24:1	648.6/264.4	0.00469187	0.00527970	0.00580492	0.00974308	0.00588159	0.00434568	0.00735487	0.00589802	0.00569442	0.00755474	0.00912197	0.00685815
Cer d18:1/26:1	676.7/264.4	0.00016757	0.00013134	0.00022701	0.00007271	0.00012955	0.00036214	0.00024214	0.00028189	0.00037180	0.00028557	0.00015818	0.00026104
GM3 d18:0/16:0	1153.6/290.1	0.00021775	0.00038338	0.00022999	0.00053586	0.00034880	0.00023227	0.00043157	0.00028483	0.00023192	0.00047316	0.00031101	0.00019934
GM3 d18:0/18:0	1181.6/290.1	0.00006798	0.00011420	0.00006644	0.00022501	0.00009737	0.00006244	0.00014551	0.00008787	0.00005271	0.00016691	0.00008985	0.00009096
GM3 d18:0/20:0	1209.6/290.1	0.00004040	0.00009245	0.00005963	0.00015738	0.00007412	0.00004246	0.00009328	0.00008333	0.00004392	0.00011791	0.00007948	0.00004064
GM3 d18:0/22:0	1237.6/290.1	0.00020691	0.00041057	0.00025895	0.00066332	0.00044762	0.00023726	0.00042162	0.00033028	0.00025124	0.00051297	0.00034557	0.00025353
GM3 d18:0/24:0	1265.6/290.1	0.00028573	0.00062945	0.00034413	0.00090524	0.00062057	0.00038212	0.00070021	0.00046663	0.00034963	0.00066457	0.00049417	0.00037352
GM3 d18:1/16:0	1151.6/290.1	0.00081187	0.00140572	0.00079728	0.00216945	0.00156959	0.00071679	0.00130092	0.00123324	0.00085212	0.00164457	0.00126306	0.00083800
GM3 d18:1/18:0	1179.6/290.1	0.00022563	0.00045951	0.00025043	0.00078038	0.00044617	0.00021229	0.00048132	0.00036815	0.00024070	0.00064619	0.00044406	0.00028256
GM3 d18:1/20:0	1207.6/290.1	0.00009065	0.00026782	0.00012777	0.00038109	0.00025724	0.00016484	0.00026864	0.00018635	0.00013177	0.00025878	0.00021080	0.00014515
GM3 d18:1/22:0	1235.6/290.1	0.00077837	0.00148593	0.00097786	0.00255314	0.00170620	0.00101150	0.00154842	0.00129535	0.00087145	0.00168132	0.00129762	0.00095799
GM3 d18:1/24:0	1263.6/290.1	0.00135574	0.00261839	0.00169849	0.00425437	0.00285723	0.00167833	0.00262423	0.00231497	0.00152503	0.00287417	0.00222721	0.00155214
GM3 d18:1/26:0	1291.6/290.1	0.00003744	0.00008973	0.00005281	0.00017689	0.00008284	0.00003996	0.00011318	0.00006515	0.00005622	0.00013628	0.00007257	0.00003484
GM3 d18:1/16:1	1149.6/290.1	0.00002956	0.00005302	0.00004259	0.00009755	0.00007557	0.00002747	0.00006467	0.00005454	0.00005622	0.00007809	0.00004492	0.00002709
GM3 d18:1/18:1	1177.6/290.1	0.00006601	0.00015362	0.00007325	0.00018469	0.00014243	0.00007493	0.00011567	0.00010757	0.00008609	0.00011791	0.00013477	0.00010064
GM3 d18:1/20:1	1205.6/290.1	0.00003350	0.00013459	0.00005622	0.00016908	0.00011336	0.00004995	0.00010572	0.00007575	0.00006149	0.00014853	0.00011058	0.00006000
GM3 d18:1/22:1	1233.6/290.1	0.00052515	0.00095709	0.00069507	0.00151003	0.00103767	0.00058692	0.00095641	0.00081357	0.00052006	0.00107035	0.00078099	0.00064060
GM3 d18:1/24:1	1261.6/290.1	0.00231047	0.00449043	0.00295574	0.00711576	0.00451692	0.00273978	0.00456318	0.00394060	0.00272855	0.00489084	0.00382375	0.00278302
GM3 d18:1/26:1	1289.6/290.1	0.00004926	0.00014003	0.00009029	0.00031475	0.00016423	0.00009990	0.00018034	0.00008484	0.00006676	0.00017456	0.00011922	0.00008903
PS 32:0	734.6/647.6	0.00204620	0.00244885	0.00304802	0.00235835	0.00278871	0.00230637	0.00310156	0.00377379	0.00355000	0.00308608	0.00314125	0.00368223
PS 34:0	762.6/675.6	0.00526884	0.00681533	0.00903373	0.00576021	0.00736220	0.00710986	0.00707655	0.00812427	0.00965931	0.00768533	0.00666992	0.00862782
PS 36:0	790.6/703.6	0.00691787	0.01017117	0.01419192	0.00843161	0.00953119	0.01120237	0.01055245	0.01105832	0.01377346	0.01039311	0.00988447	0.01375829
PS 32:1	732.6/645.6	0.00954223	0.01125955	0.01355749	0.01012211	0.01313793	0.00990178	0.01361836	0.01447800	0.01775001	0.01031347	0.01030330	0.01209435
PS 34:1	760.6/673.6	0.05207504	0.06508250	0.08506875	0.04729216	0.06823045	0.06518527	0.06379595	0.07172226	0.09201112	0.06072606	0.06142194	0.07848231
PS 36:1	788.6/701.6	0.06036039	0.08602085	0.12701007	0.07888983	0.08689622	0.10104671	0.10023040	0.09458759	0.12996036	0.09783864	0.08961991	0.12325451
PS 38:1	816.6/729.6	0.00241824	0.00378342	0.00572366	0.00394449	0.00360673	0.00440465	0.00561490	0.00342980	0.00554516	0.00537575	0.00374856	0.00488396
PS 34:2	758.6/671.6	0.00699328	0.00843494	0.01268859	0.00692895	0.00879993	0.00958964	0.01048115	0.01119996	0.01514943	0.00953698	0.00930858	0.01157052
PS 36:2	786.6/699.6	0.02717877	0.03786006	0.05457475	0.03739962	0.03834787	0.04527766	0.05493688	0.04026726	0.06021245	0.04909851	0.03874210	0.05820694

PS 38:2	814.6/727.6	0.00415776	0.00656915	0.00946128	0.00686634	0.00681685	0.00795957	0.01192498	0.00573657	0.01034729	0.01220495	0.00593697	0.00966007
PS 38:3	812.6/725.6	0.00379578	0.00623227	0.00903373	0.00826465	0.00565179	0.00619078	0.01210323	0.00542293	0.00915020	0.01552995	0.00668040	0.01092343
PS 40:4	838.6/751.6	0.00108594	0.00230633	0.00315835	0.00375666	0.00229294	0.00235839	0.00716568	0.00135573	0.00305465	0.00812335	0.00188475	0.00415984
PS 40:5	836.6/749.6	0.00426334	0.00796849	0.01137836	0.01682148	0.00762248	0.00988444	0.02900140	0.00490694	0.01261764	0.03297126	0.00615685	0.01500624
PS 40:6	834.6/747.6	0.00409240	0.00812398	0.01068876	0.01554839	0.00668051	0.00816767	0.02698716	0.00447189	0.01087016	0.03528084	0.00657569	0.01409724
PI 34:0	837.6/241.1	0.00043731	0.00104710	0.00150144	0.00064213	0.00112853	0.00164174	0.00103776	0.00128372	0.00181817	0.00100307	0.00120978	0.00182658
PI 34:1	835.5/241.1	0.00310561	0.00759705	0.01072027	0.00462676	0.00827750	0.01204976	0.00623625	0.00969627	0.01275707	0.00647975	0.00841592	0.01327924
PI 36:1	863.6/241.1	0.00672158	0.01489631	0.01785398	0.00809193	0.01613940	0.01864770	0.01258072	0.01674444	0.02126444	0.01196447	0.01511832	0.02029830
PI 36:2	861.6/241.1	0.00845998	0.02128936	0.02614380	0.01140441	0.02236846	0.02573844	0.01702309	0.02636003	0.03210178	0.01690907	0.02291185	0.03069044
PI 36:3	859.6/241.1	0.00079861	0.00237918	0.00287338	0.00106370	0.00239996	0.00259074	0.00181607	0.00281120	0.00356465	0.00201899	0.00275409	0.00370344
PI 38:3	887.6/241.1	0.00188943	0.00518745	0.00637736	0.00271210	0.00558678	0.00625157	0.00410663	0.00659395	0.00771080	0.00458935	0.00643010	0.00846501
PI 38:4	885.6/241.1	0.00223099	0.00600559	0.00800267	0.00266381	0.00627671	0.00694994	0.00518878	0.00813897	0.00858902	0.00636562	0.00887105	0.01084220
PI 40:4	913.6/241.1	0.00023396	0.00052355	0.00098344	0.00034195	0.00064558	0.00103348	0.00079497	0.00069622	0.00108732	0.00088251	0.00085774	0.00122091
PI 38:5	883.6/241.1	0.00123198	0.00316050	0.00432977	0.00148265	0.00356299	0.00401002	0.00325617	0.00479640	0.00485111	0.00385956	0.00489551	0.00605669
PI 40:5	911.6/241.1	0.00042942	0.00094303	0.00180548	0.00061081	0.00104803	0.00160795	0.00134020	0.00126969	0.00186198	0.00165088	0.00153653	0.00221919
PI 38:6	881.6/241.1	0.00045015	0.00088699	0.00116925	0.00049465	0.00107760	0.00114049	0.00110296	0.00116797	0.00156725	0.00115899	0.00118838	0.00142919
PE 32:0a	690.6/196.1	0.01042004	0.00468319	0.00430586	0.00441342	0.00447040	0.00500325	0.00332218	0.00464706	0.00359559	0.00401434	0.00425955	0.00450085
PE 34:0a	718.6/196.1	0.01135785	0.00523666	0.00440920	0.00612474	0.00494096	0.00516820	0.00418203	0.00502797	0.00388556	0.00376080	0.00471892	0.00439283
PE 32:1a	688.6/196.1	0.03636594	0.02426746	0.01808462	0.02449897	0.02544988	0.02358678	0.01903411	0.02411140	0.01644113	0.01757857	0.01904271	0.01602301
PE 34:1a	716.6/196.1	0.08461072	0.03767842	0.03227673	0.04192746	0.03999827	0.03766187	0.03126753	0.03850967	0.02995360	0.02810036	0.03482812	0.02714910
PE 36:1a	744.6/196.1	0.04980779	0.02443776	0.02063368	0.02382345	0.02454796	0.02331187	0.01860418	0.02133078	0.01907984	0.01867723	0.01937679	0.01926362
PE 34:2a	714.6/196.1	0.04918258	0.02452290	0.02111594	0.02314792	0.02286176	0.02243218	0.01657179	0.02338767	0.01881886	0.01686022	0.02079665	0.01508683
PE 36:2a	742.6/196.1	0.10930622	0.04457549	0.03692706	0.04462956	0.05156640	0.04326992	0.03591858	0.04601353	0.03476706	0.03908697	0.04079984	0.03737502
PE 36:3a	740.6/196.1	0.01594266	0.00936639	0.00861172	0.01022292	0.00972507	0.00929176	0.00750421	0.00975121	0.00794510	0.00887380	0.01039832	0.00918173
PE 38:3a	768.6/196.1	0.00906544	0.00553468	0.00492590	0.00432335	0.00454882	0.00346379	0.00426020	0.00582787	0.00318964	0.00477495	0.00547060	0.00532900
PE 38:4a	766.6/196.1	0.00750243	0.01583771	0.01388210	0.01706822	0.01419547	0.01352528	0.01407039	0.01573145	0.01191765	0.01512772	0.01753934	0.01411465
PE 40:4a	794.6/196.1	0.00072940	0.00076634	0.00086117	0.00094573	0.00117642	0.00098965	0.00109436	0.00083800	0.00081191	0.00088738	0.00104401	0.00111621
PE 38:5a	764.6/196.1	0.00427222	0.01158026	0.01009294	0.01071830	0.00999957	0.00989655	0.01008378	0.01017021	0.00939493	0.01039502	0.01223578	0.01101807
PE 40:5a	792.6/196.1	0.00218821	0.00468319	0.00341024	0.00522405	0.00435275	0.00423353	0.00328309	0.00422806	0.00292867	0.00342275	0.00505300	0.00439283
PE 34:0p	702.6/196.1	0.01312925	0.00502379	0.00330690	0.00472866	0.00388219	0.00324387	0.00386936	0.00453279	0.00345061	0.00371854	0.00396723	0.00331262
PE 34:1p	700.6/196.1	0.03782475	0.01494364	0.01178084	0.01405088	0.01411704	0.01358027	0.00984927	0.01424591	0.01183066	0.00900057	0.01373915	0.01087404
PE 36:1p	728.6/196.1	0.01062844	0.00604558	0.00465033	0.00612474	0.00643109	0.00549808	0.00437746	0.00639923	0.00455248	0.00392983	0.00551236	0.00518497
PE 36:2p	726.6/196.1	0.00927383	0.01081392	0.00840504	0.01139382	0.01058778	0.00896188	0.00801231	0.01009403	0.00782911	0.00671873	0.00793446	0.00691330
PE 38:2p	754.6/196.1	0.00291761	0.00119209	0.00175679	0.00189147	0.00152935	0.00126456	0.00097711	0.00163790	0.00095689	0.00126769	0.00141985	0.00118822
PE 36:3p	724.6/196.1	0.00312601	0.00570498	0.00406473	0.00535915	0.00533310	0.00560804	0.00418203	0.00506606	0.00414653	0.00452141	0.00451012	0.00403276
PE 38:3p	752.6/196.1	0.00541842	0.00251189	0.00179124	0.00207161	0.00223520	0.00230919	0.00164154	0.00213308	0.00246472	0.00202830	0.00229682	0.00154829
PE 38:4p	750.6/196.1	0.00458482	0.00813173	0.00706161	0.00648502	0.00729380	0.00615785	0.00672252	0.00864658	0.00698821	0.00667648	0.00709926	0.00795749
PE 40:4p	778.6/196.1	0.00187560	0.00153268	0.00106785	0.00121594	0.00141170	0.00098965	0.00078169	0.00144745	0.00147883	0.00152122	0.00121105	0.00104420
PE 38:5p	748.6/196.1	0.00354281	0.01907337	0.01419212	0.01522179	0.01658752	0.01473486	0.01274152	0.01740744	0.01478832	0.01512772	0.01603597	0.01562693
PE 40:5p	776.6/196.1	0.00312601	0.00234160	0.00289354	0.00238685	0.00294105	0.00208927	0.00285316	0.00289489	0.00266770	0.00270439	0.00300674	0.00266450
PE 38:6p	746.6/196.1	0.00875283	0.01311294	0.00864617	0.01197928	0.01458760	0.01055632	0.01059188	0.01173193	0.01011985	0.01200076	0.01261162	0.01098206
PE 40:6p	774.6/196.1	0.00281341	0.00570498	0.00509814	0.00603467	0.00596053	0.00483831	0.00551090	0.00457088	0.00536439	0.00405659	0.00517828	0.00572507
	PC	0.23647298	0.28587743	0.22092664	0.31046054	0.27631981	0.27556457	0.26726976	0.25803315	0.19594144	0.26447172	0.29053326	0.20591164
	SM	0.02147902	0.03002287	0.03657694	0.03284697	0.03093808	0.03806009	0.02923226	0.03950349	0.03847327	0.02507779	0.04242036	0.03700412
	GlcCer	0.00789502	0.01508359	0.00749054	0.01550053	0.01376363	0.00903732	0.01345396	0.00924646	0.00945942	0.01131566	0.01055391	0.01006773
	Cer	0.01307022	0.01883356	0.02159820	0.02646627	0.01741159	0.01506504	0.02354770	0.02094666	0.01780728	0.02359883	0.03029232	0.02411032
	GM3	0.00713241	0.01388592	0.00877693	0.02219398	0.01455790	0.00835920	0.01411489	0.01179302	0.00812590	0.01565710	0.01184965	0.00846904
	PS	0.19019607	0.26307689	0.36861745	0.25238485	0.26776578	0.29058516	0.35659063	0.28053531	0.39365126	0.35816431	0.26007470	0.36840775
	PI	0.02598901	0.06391611	0.08176084	0.03413491	0.06851153	0.08166182	0.05448360	0.07955887	0.09717359	0.05688226	0.07418926	0.10003120
	PE	0.49776528	0.30930363	0.25425246	0.30601195	0.31073168	0.28166679	0.24130720	0.30038306	0.23936785	0.24483233	0.28008654	0.24599819

Dark brown shading: ceramide lipids that were found to be significantly upregulated in HAdV-C2 infected cells.

Light brown shading: marginally upregulated ceramide lipids in HAdV-C2 infected cells.

Supplemental Videos

Video 1: Ca^{2+} transients in HAdV-C2 inoculated cells: GCamP (green cytoplasm) and HAdV-C2-Atto565 (grey) (related to Fig. 6).

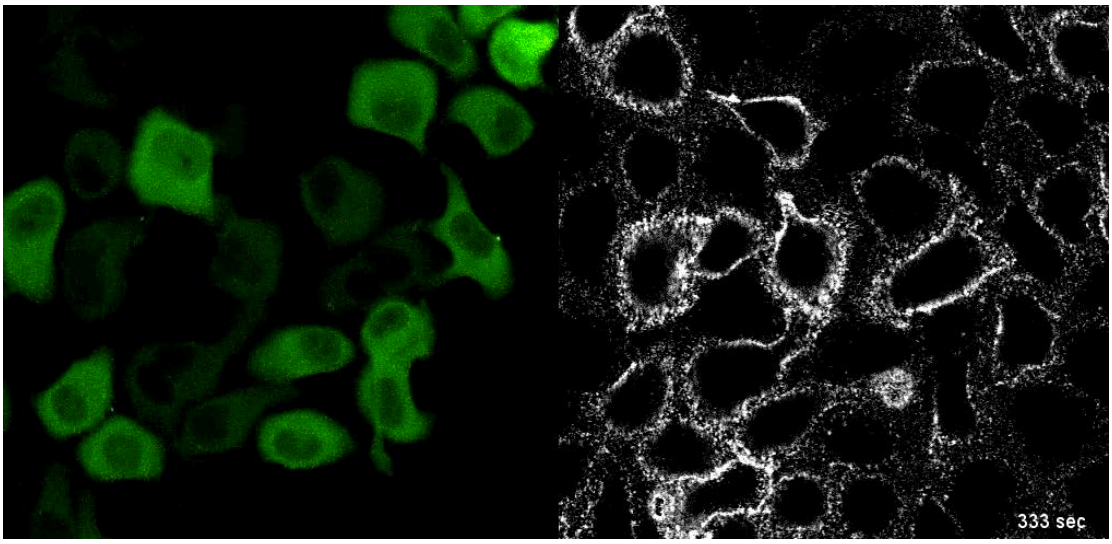

Video 2: Ca^{2+} transients and propidium iodide influx into HAdV-C2 inoculated cells: GCamP (green cytoplasm) and propidium iodide (gray) (related to Fig. 6).

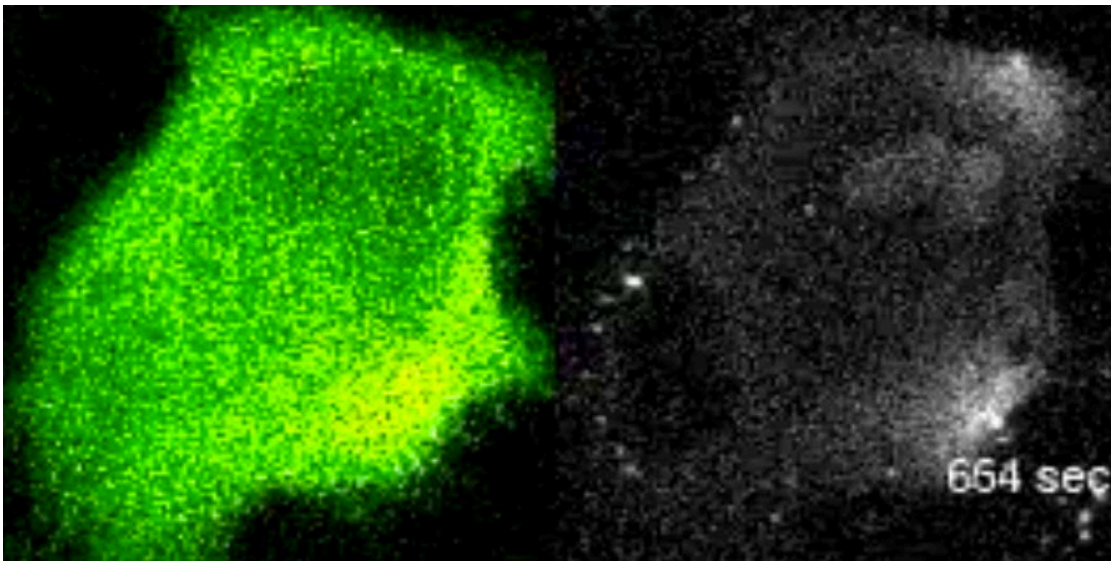

Video 3: No Ca^{2+} transients in TS1 inoculated cells: GCamP (green cytoplasmic signal) and TS1-Alexa488 (green puncta) (related to Fig. 6).

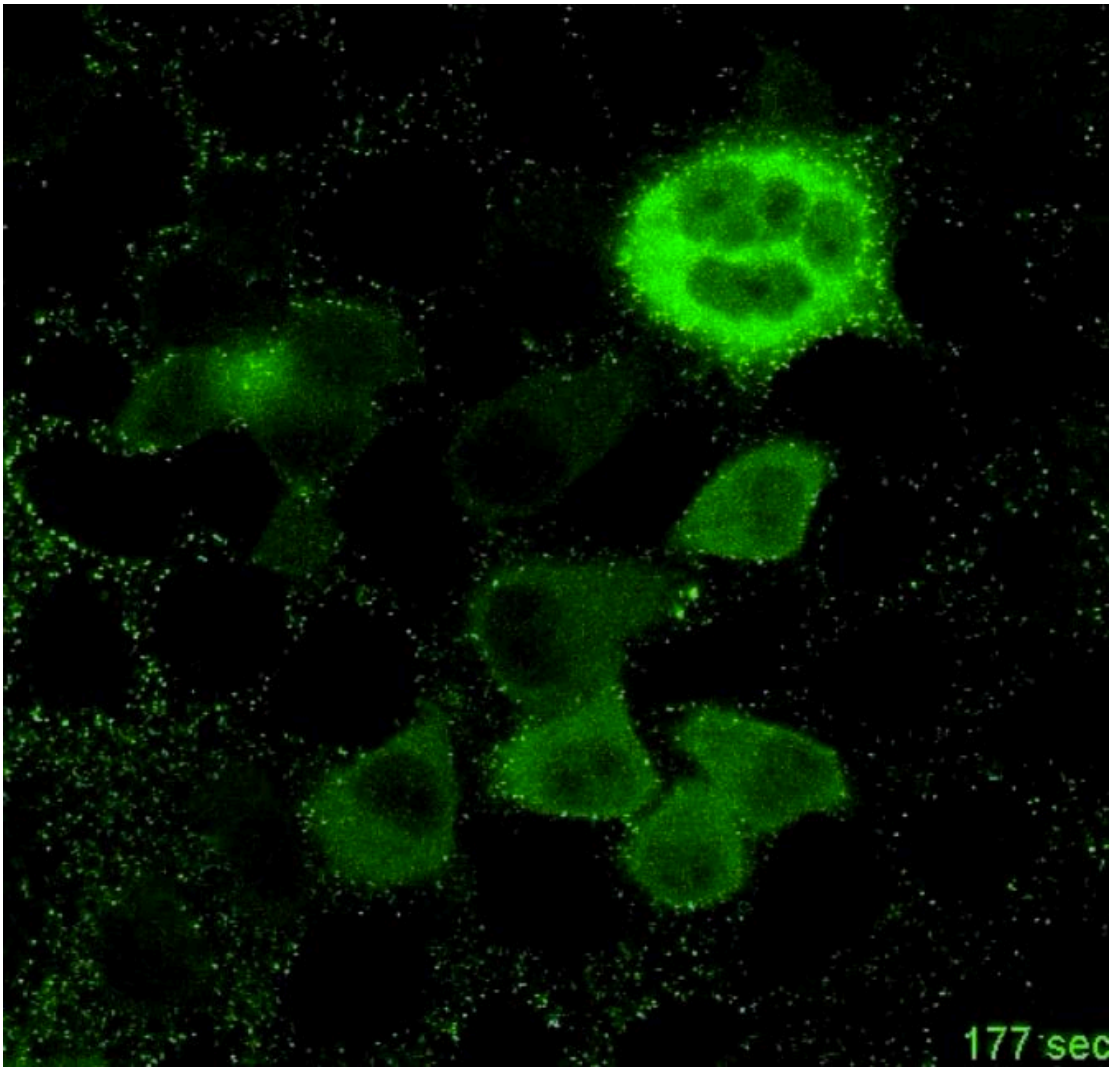

Video 4: No Ca^{2+} transients in EDTA medium: GCamP (green cytoplasm) and HAdV-C2-Atto565 (grey) (related to Fig. 6).

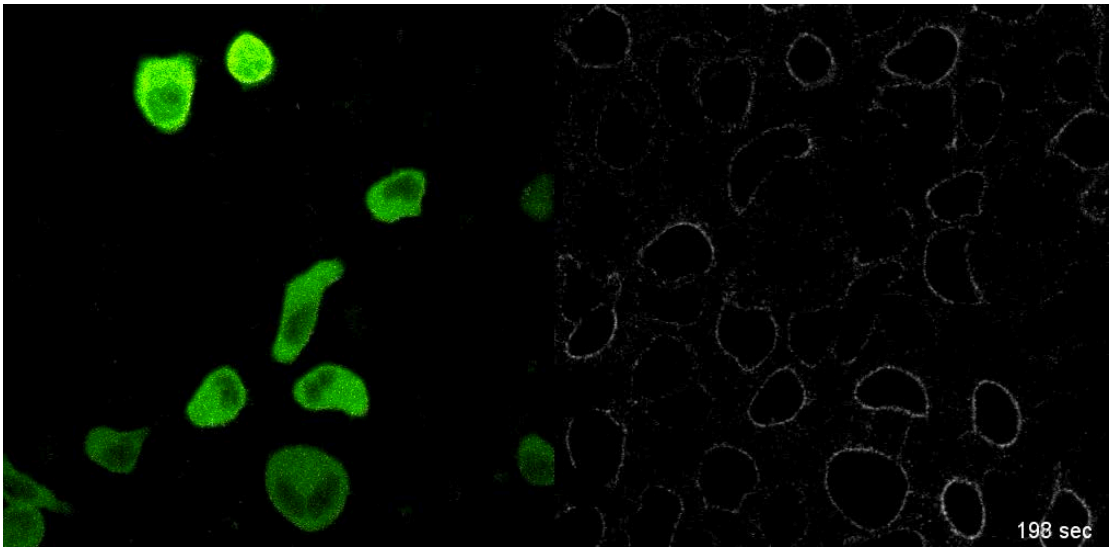

Video 5: HAdV-C2 induced blebbing and massive Ca^{2+} influx: GCamP (green cytoplasm) and propidium iodide (grey) (related to Fig. 6).

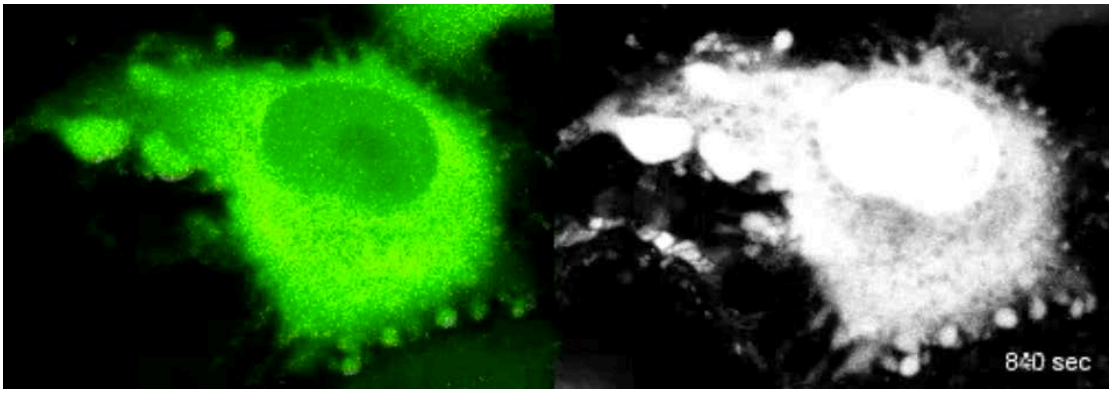

Supplemental Video Legends

Videos 1,3,4: Incoming HAdV-C2-Atto565 but not TS1-Atto488 induce cytosolic Ca^{2+} transients, depending on extracellular Ca^{2+}

Cells expressing the Ca^{2+} sensor GCamP in the cytosol (green) were imaged during the first minutes of infection with HAdV-C2-Atto565 (videos 1, 4) or TS1-Atto488 (video 3) in medium with (video 1, 3) or without extracellular Ca^{2+} (video 4). Cytosolic Ca^{2+} transients are observed only when incoming, uncoating competent viruses infect cells in presence of extracellular Ca^{2+}.

Videos 2,5: Cytosolic Ca^{2+} transients are a consequence of plasma membrane permeabilization

Cells expressing cytosolic GCamP (green) were imaged during infection with HAdV-C2 in presence of the membrane impermeant dye propidium iodide (0.2 mg/ml). Cytosolic Ca^{2+} transients occurred simultaneously with the influx of PI. Ca^{2+} and PI influxes are mostly transient (video 2) but in rare cases, they are unresolved and induce plasma membrane blebbing (video 5).

Supplemental References

Baum, S.G., Horwitz, M.S., and J.V. Maizel, J. (1972). Studies of the mechanism of enhancement of human adenovirus infection in monkey cells by simian virus 40. J Virol *10*, 211-219.

Burckhardt, C.J., Suomalainen, M., Schoenenberger, P., Boucke, K., Hemmi, S., and Greber, U.F. (2011). Drifting motions of the adenovirus receptor CAR and immobile integrins initiate virus uncoating and membrane lytic protein exposure. Cell Host Microbe *10*, 105-117.

Czekanska, E.M. (2011). Assessment of cell proliferation with resazurin-based fluorescent dye. Methods Mol Biol *740*, 27-32.

Ebbinghaus, C., Al-Jaibaji, A., Operschall, E., Schoffel, A., Peter, I., Greber, U.F., and Hemmi, S. (2001). Functional and selective targeting of adenovirus to high-affinity Fcgamma receptor I-positive cells by using a bispecific hybrid adapter. J Virol *75*, 480-489.

Evans, M.J., Eddy, M., and Plummer, J. (1985). A comparative assessment of lactate dehydrogenase isozymes, LDHk and LDH5. J Biol Chem *260*, 306-314.

Fleischli, C., Sirena, D., Lesage, G., Havenga, M.J., Cattaneo, R., Greber, U.F., and Hemmi, S. (2007). Species B adenovirus serotypes 3, 7, 11 and 35 share similar binding sites on the membrane cofactor protein CD46 receptor. J Gen Virol *88*, 2925-2934.

Greber, U.F., Suomalainen, M., Stidwill, R.P., Boucke, K., Ebersold, M., and Helenius, A. (1997). The role of the nuclear pore complex in adenovirus DNA entry. EMBO J *16*, 5998-6007.

Greber, U.F., Webster, P., Weber, J., and Helenius, A. (1996). The role of the adenovirus protease on virus entry into cells. EMBO J *15*, 1766-1777.

Greber, U.F., Willetts, M., Webster, P., and Helenius, A. (1993). Stepwise dismantling of adenovirus 2 during entry into cells. Cell *75*, 477-486.

Moyer, C.L., Wiethoff, C.M., Maier, O., Smith, J.G., and Nemerow, G.R. (2011). Functional genetic and biophysical analyses of membrane disruption by human adenovirus. J Virol *85*, 2631-2641.

Nagel, H., Maag, S., Tassis, A., Nestle, F.O., Greber, U.F., and Hemmi, S. (2003). The alphavbeta5 integrin of hematopoietic and nonhematopoietic cells is a transduction receptor of RGD-4C fiber-modified adenoviruses. Gene Ther *10*, 1643-1653.

Rodríguez, A., Webster, P., Ortego, J., and Andrews, N.W. (1997). Lysosomes behave as Ca2+-regulated exocytic vesicles in fibroblasts and epithelial cells. J Cell Biol *137*, 93-104.

Sirena, D., Ruzsics, Z., Schaffner, W., Greber, U.F., and Hemmi, S. (2005). The nucleotide sequence and a first generation gene transfer vector of species B human adenovirus serotype 3. Virology *343*, 283-298.

Suomalainen, M., Luisoni, S., Boucke, K., Bianchi, S., Engel, D.A., and Greber, U.F. (2013). A direct and versatile assay measuring membrane penetration of adenovirus in single cells. J Virol *87*, 12367-12379.

Tanner, L.B., Chng, C., Guan, X.L., Lei, Z., Rozen, S.G., and Wenk, M.R. (2014). Lipidomics identifies a requirement for peroxisomal function during influenza virus replication. J Lipid Res *55*, 1357-1365.

van Diggelen, O.P., Voznyi, Y.V., Keulemans, J.L., Schoonderwoerd, K., Ledvinova, J., Mengel, E., Zschiesche, M., Santer, R., and Harzer, K. (2005). A new fluorimetric enzyme assay for the diagnosis of Niemann-Pick A/B, with specificity of natural sphingomyelinase substrate. J Inherit Metab Dis *28*, 733-741.

Varghese, R., Mikyas, Y., Stewart, P.L., and Ralston, R. (2004). Postentry neutralization of adenovirus type 5 by an antihexon antibody. J Virol *78*, 12320-12332.

Yakimovich, A., Gumpert, H., Burckhardt, C.J., Lutschg, V.A., Jurgeit, A., Sbalzarini, I.F., and Greber, U.F. (2012). Cell-free transmission of human adenovirus by passive mass transfer in cell culture simulated in a computer model. J Virol *86*, 10123–10137.